

NATIONAL TSING HUA UNIVERSITY

MASTER'S THESIS

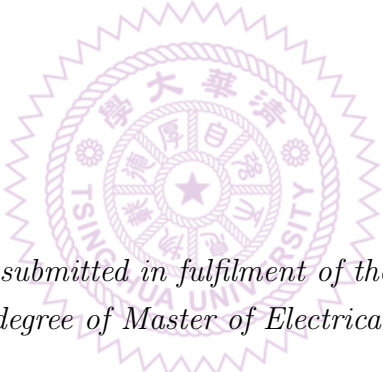
Simulating Masking and Anti-masking Effects of the Medial Olivocochlear Efferent Reflex

Author:

Po-Jui Wu

Supervisor:

Dr. Yi-Wen LIU



*A thesis submitted in fulfillment of the requirements
for the degree of Master of Electrical Engineering
in the*

Department of Electrical Engineering

November 2014

NATIONAL TSING HUA UNIVERSITY

Abstract

Master of Electrical Engineering

Simulating Masking and Anti-masking Effects of the Medial Olivocochlear Efferent Reflex

by Po-Jui Wu

The masking effect happens when the background noise influences the target sound, which is then difficult to be perceived. To simulated this effect, we constructed a tone-burst-in-noise stimulus, and then fed into the model comprised of middle ear, cochlear membrane-fluid system, outer hair cell (OHC), inner hair cell (IHC), auditory nerve (AN), T-multipolar (TM) cell. This model successfully simulated the masking effect especially in low-level region. The medial olivocochlear reflex (MOCR), a descending auditory pathway, induces the anti-masking effect to reduce the masking effect and help human to perceive sounds. Based on an experiment of the OHC which showed the conductance of OHC was increased after applying acetylcholine (ACh), we have constructed the MOC model by changing the conductance of OHC and simulated the anti-masking effect. The tuberculoventral (TUB) cell is an inhibitory interneuron in dorsal cochlear nucleus (DCN) and projects to the ventral cochlear nucleus (VCN). The TUB inhibits the interneuron in VCN, and is sensitive to tones, while not to noise. We have used these two properties to construct a TUB model and enhance the anti-masking effect in sustained tone-in-noise conditions.

Acknowledgements

This project about the masking and anti-masking effects is really an advanced and challenging research for a electrical engineering background student like me.

I have to especially thank to my advisor, Dr. Yi-Wen Liu, who brings me to a new field of computer simulation in physiology. He is also my advisor of special topic on implementation, which is about acoustic signal processing, while I was a undergraduate. When I entered the graduate school, Dr. Liu assigned me to a new topic about computer simulation of masking effect, rather than continue the audio topic. I appreciate to be involved and take this challenge, so that I can peek into the depth of the human hearing system. Thanks to the reading club, it is very helpful to build the basic hearing knowledge from the ground up.

I have to also thank to Lu-Ming Yu, a graduated acoustic and hearing group (AHG) member. he is a pioneer researching the hearing topics in AHG. Without the models he had studied and established, I would never continue his work and achieve the current progress.

I want to thank to all the AHG members, who bring me the joy in these two years. It is an unforgettable experience joining the group meetings, tidying the laboratory up, and watching the advancement of AHG.

Contents

| | |
|---|------------|
| Abstract | i |
| Acknowledgements | ii |
| Contents | iii |
| List of Figures | v |
| List of Tables | vi |
| Abbreviations | vii |
| 1 Introduction | 1 |
| 1.1 Motivation | 1 |
| 1.2 Background | 3 |
| 1.2.1 What is a Biophysical Model? | 3 |
| 1.2.2 Research Method | 4 |
| 1.2.3 Liu and Neely Model [1][2] - Middle Ear, Basilar Membrane, and Outer Hair Cell | 4 |
| 1.2.4 Sumner et al. Model [3] - Inner Hair Cell and Auditory Nerve | 5 |
| 1.2.5 Hewitt et al. Model [4] - T-Multipolar Cell | 5 |
| 1.2.6 Thesis Organization | 6 |
| 2 Peripheral Auditory System | 7 |
| 2.1 Outer Ear | 7 |
| 2.2 Middle Ear | 8 |
| 2.3 Inner Ear | 10 |
| 2.3.1 Cochlear System | 10 |
| 2.3.2 Place Theory | 12 |
| 2.3.3 Outer Hair Cell | 14 |
| 2.3.4 OHC Mechanoelectrical Transduction | 14 |
| 2.3.5 OHC Electromotility | 14 |
| 2.3.6 State-space Formulation | 15 |
| 2.3.7 Inner Hair Cell | 16 |
| 2.3.8 IHC Model | 17 |
| 2.3.8.1 IHC Receptor Potential | 17 |
| 2.3.8.2 Calcium Controlled Transmitter Release Function | 19 |

| | | |
|----------|---|-----------|
| 2.3.8.3 | Quantal and Probabilistic Model of Synaptic Adaptation | 20 |
| 2.3.9 | Auditory Nerve | 21 |
| 3 | Higher Auditory Pathway | 22 |
| 3.1 | Masking Effects | 22 |
| 3.1.1 | Model Structure | 24 |
| 3.1.2 | Simulation Setup | 25 |
| 3.1.3 | Experiment Result | 25 |
| 3.2 | Cochlear Nucleus | 26 |
| 3.2.1 | Dendrite Model | 27 |
| 3.2.2 | Soma Model | 28 |
| 3.3 | Anti-Masking Effects | 29 |
| 3.3.1 | Experiment results of the article: Feedback Control of The Auditory Periphery: Anti-masking Effects of Middle Ear Muscles VS. Olivocochlear Efferents [5] | 30 |
| 3.3.2 | Construction of an MOC Model to Simulate the Anti-masking Effect | 32 |
| 3.3.3 | Experiment Result | 35 |
| 3.4 | The Tuberculoventral Cell | 35 |
| 3.4.1 | Construction of a TUB Model | 37 |
| 3.4.2 | Inhibiting the TM interneuron in the VCN | 38 |
| 3.4.3 | Lateral Inhibition | 38 |
| 3.5 | Simulate Sustained Tone-in-Noise Condition | 40 |
| 3.5.1 | Stimulus Setting | 40 |
| 3.5.2 | Experiment Results | 40 |
| 4 | Conclusion | 43 |
| 4.1 | Conclusion | 43 |
| 4.2 | Future Work | 43 |
| A | Parameters | 45 |
| B | State-space Formulation of Liu and Neely Model | 49 |
| B.1 | Equation (2.19) | 49 |
| B.2 | Equation (2.22) | 49 |
| B.3 | Equation (2.21) | 50 |
| B.4 | Equation (2.20) | 50 |
| | Bibliography | 52 |

List of Figures

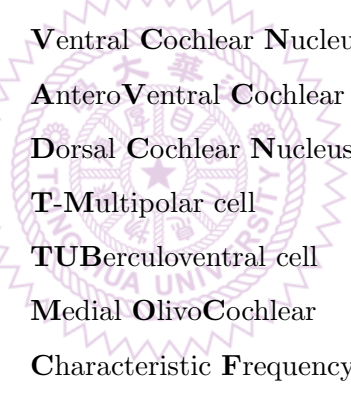
| | | |
|------|--|----|
| 1.1 | Basic Hodgkin-Huxley Model | 3 |
| 1.2 | Basic Hodgkin-Huxley Model [3] | 5 |
| 2.1 | Anatomy of the Human Ear | 8 |
| 2.2 | Matthews' Middle Ear Model [2] | 9 |
| 2.3 | Cross Section through the Cochlea [6] | 11 |
| 2.4 | Place Theory [7] | 13 |
| 2.5 | OHC Model [1] | 14 |
| 2.6 | Inner Hair Cell | 16 |
| 2.7 | IHC Membrane Potential Model | 18 |
| 2.8 | Meddis Model | 20 |
| 3.1 | Masking Audiograms | 23 |
| 3.2 | Model Diagram | 24 |
| 3.3 | Spatial Quantization Index | 25 |
| 3.4 | Stimulus | 26 |
| 3.5 | RL Plot of AN at Tone Burst in Noise condition | 27 |
| 3.6 | MEM Reflex Loop [5] | 30 |
| 3.7 | MOC Reflex Loops [5] | 30 |
| 3.8 | Comparison of MEM and MOC peripheral effects [5] | 31 |
| 3.9 | Excitatory Masking [5] | 32 |
| 3.10 | Suppressive Masking [5] | 32 |
| 3.11 | MEM Anti-Masking [5] | 33 |
| 3.12 | MOC Anti-Masking [5] | 33 |
| 3.13 | Outer hair cell responses to ACh [8] | 34 |
| 3.14 | MOC Convolution Kernel | 35 |
| 3.15 | Tuberculoventral Cell Response Characteristics [9] | 36 |
| 3.16 | TUB Convolution Kernel | 39 |
| 3.17 | Lateral Inhibition Diagram | 39 |
| 3.18 | RL Plot of AN at Sustained Tone in Noise condition | 41 |

List of Tables

| | | |
|-----|-------------------------------|----|
| A.1 | Middle Ear Parameters | 45 |
| A.2 | Chochlea and OHC Parameters | 46 |
| A.3 | IHC Parameters | 47 |
| A.4 | AN Parameters | 47 |
| A.5 | TM Cell Parameters | 48 |
| A.6 | TUB Cell Parameters | 48 |
| A.7 | Convolution Kernel Parameters | 48 |



Abbreviations



| | |
|-------------|---|
| BM | B asilar M embrane |
| IHC | I nnear H air C ell |
| OHC | O uter H air C ell |
| AN | A uditory N erve |
| CN | C ochlear N ucleus |
| VCN | V entral C ochlear N ucleus |
| AVCN | A ntero V entral C ochlear N ucleus |
| DCN | D orsal C ochlear N ucleus |
| TM | T - M ultipolar cell |
| TUB | TUB erculoventral cell |
| MOC | M edial O livo C ochlear |
| CF | C haracteristic F requency |
| AP | A ction P otential |
| IPSP | I nhibitory P ost S ynaptic P otentials |

Chapter 1

Introduction

1.1 Motivation

It is difficult to study the physiological basis of psychoacoustical phenomena. The current experiments are conducted by designing different stimulation sounds, and ask the subject whether he or she can hear them or tell the difference. For example, in an equal-loudness experiment, the listener is asked if the presented tone is equally loud as a 1000 Hz reference tone. For another example, in an auditory masking experiment, the listener is asked if he/she is able to hear the tone when the masker is presented. However, it is not convenient to study the physiological basis of hearing. On one hand, it is illegal and impossible to conduct the surgery, like decerebration, on human beings. On the other hand, if the experiments are conducted on non-human animals, they still cannot answer subjective questions.

Thereupon, we are trying to approach the experiments by using another method, computer simulation. First, by using the biology experiment results, several models are constructed. These models can be any forms, e.g., they can be some parts of a cell, neurons, or even only functions. Second, these models are joined and connected properly, that is the output of one model are connected to the input of another. Finally, the stimulus signals are generated and fed into the models. After some computer calculations, the outputs are obtained and analyzed.

The auditory model from the middle ear to the T-multipolar (TM) cells has been constructed before by Yu [10] for the purpose of simulating the auditory masking and

anti-masking phenomenon. The model structures are described as following. Yu [10] adopted Liu and Neely model [2] from the middle ear to the outer hair cells (OHC) in the cochlea. Liu and Neely used mechanical components to simulate middle ear mechanism, fluid mechanics to simulate the membrane-fluid conduction in the cochlea, and electrical components to simulate the OHC functions. They supposed that the transduction current is a nonlinear function of basilar membrane (BM) displacement, and then successfully simulated the distortion product emissions. The inner hair cells (IHC) and auditory nerves (AN) model is adapted from Sumner et al.'s work [3]. The original model used some filtering methods to transform the input sound into the BM movement to describe the transduction activities in the IHC and AN. Yu adapted the IHC and AN parts of the model. The TM cells model is adopted from Hewitt et al [4]. Hewitt used differential equations to describe the cell activity in the soma, and low-pass filtering to simulate the dendritic current.

Based on the hearing models described in the last paragraph, we want to simulate psychophysical phenomena in the human hearing system. Our interest is to simulate auditory masking and anti-masking. Kawase et al. [11] have recorded the AN spiking rate in different conditions of medial olivocochlear reflex (MOCR). Chintanpalli et al. [12] conducted the open-loop simulations, and simulated the anti-masking effects based on Kawase et al's experiment results. However, their models are based on some filtering technique, and they changed the OHC gain by adjusting the OHC parameter. We then want to further use the biophysical model to simulated the closed-loop simulation, which is more realistic to biology basis. Housley and Ashmore [8]'s experiment results showed that the acetylcholine (ACh), which is a neurotransmitter for the medial olivocochlea (MOC) reflex, changes the conductance of the OHC. Therefore, we establish the MOC model and conduct the closed-loop simulations by adjusting the OHC conductance to simulate the anti-masking effects. Finally, we proposed an tuberculoventral (TUB) cell model to inhibit the TM cell and reduce the anti-masking effect. The TUB model then is found to smooth the rate-level (RL) curves of the AN.

1.2 Background

1.2.1 What is a Biophysical Model?

One of the earliest and most famous computer models in biology is the Hodgkin–Huxley model [13]. In 1952, Alan Lloyd Hodgkin and Andrew Huxley used nonlinear differential equations to describe how an action potential in a neuron is initiated and propagated. They collected data from the squid giant axon, and built up their model by considering electrical characteristics.

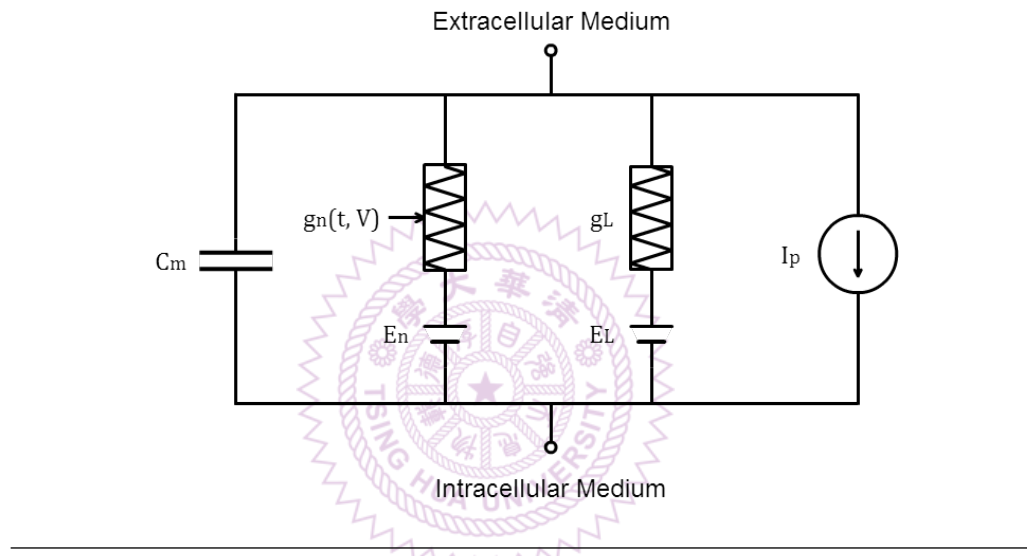


FIGURE 1.1: Basic Hodgkin-Huxley Model

Figure 1.1 is a basic Hodgkin–Huxley-type model. The lipid layer is characterized by a capacitance (C_m). Voltage-gated channels and leakage ion channels are characterized by nonlinear conductance (g_n) and linear conductances (g_L), respectively. The reversal potentials are characterized by single cells (E_n and E_L). Ion pumps and exchangers are characterized by current sources (I_p).

The conductance-based model transform the complicated physiological phenomenon into simple electrical components; therefore, it is quite intuitive for people with electrical engineering background to understand it. Also, the calculation complexity is low. We can easily simulate the model by using personal computers without expensive equipments.

1.2.2 Research Method

The research in this work is based upon Yu's research [10], which combined many well-constructed models and established a large biophysical auditory model from the middle ear to the cochlea nucleus (CN). The auditory model divides into four parts:

- Liu and Neely Model [1][2] - middle ear, basilar membrane, and outer hair cell
- Sumner et al. Model [3] - inner hair cell and auditory nerve
- Hewitt et al. Model [4] - T-multipolar cell
- tuberculoventral cell [10]

The first three parts are adopted in this work, and a new medial olivocochlear (MOC), and tuberculoventral cell (TUB) model are added to simulate networked activities in the auditory brainstem. The auditory nerves (AN) serve as the output of peripheral auditory system, and the outer hair cells (OHC) are then mediated by the descending pathway from the central auditory system.

The objective is to simulate the masking and anti-masking effect in human hearing system. The masking effect can be simulated by pre-introducing a long noise duration (300ms) to deplete the neuron transmitters in the IHC; therefore, the IHC becomes insensitive to tones. The anti-masking effect is simulated by adding in a closed-loop MOC model which adjusts the conductance of the OHC, and later is enhanced in a tone-in-noise condition by joining a TUB model which inhibits the TM cell and also TUB cells.

1.2.3 Liu and Neely Model [1][2] - Middle Ear, Basilar Membrane, and Outer Hair Cell

Liu and Neely Model [1][2] includes stimulus input, middle ear mechanism [14], mechano-electrical transduction and electromotility of OHC, and cochlear macromechanics. The main purpose of this model is to construct a nonlinear mechano-electrical transduction mechanism of OHC to simulate distortion product otoacoustic emissions (DPOAE) [2]. From Yu's previous work [10], he adopted this model to input the sounds and acquire the BM velocity.

1.2.4 Sumner et al. Model [3] - Inner Hair Cell and Auditory Nerve

Sumner et al. model [3] contains several parts: middle ear, dual resonance nonlinear (DRNL) cochlear filtering [15], IHC model [16], and AN response. Yu adopted the IHC, and AN parts as Figure 1.2 [3] shows. He used the BM velocity, which is the output of Liu and Neely model, as the input of IHC, then received the outputs of ANs.

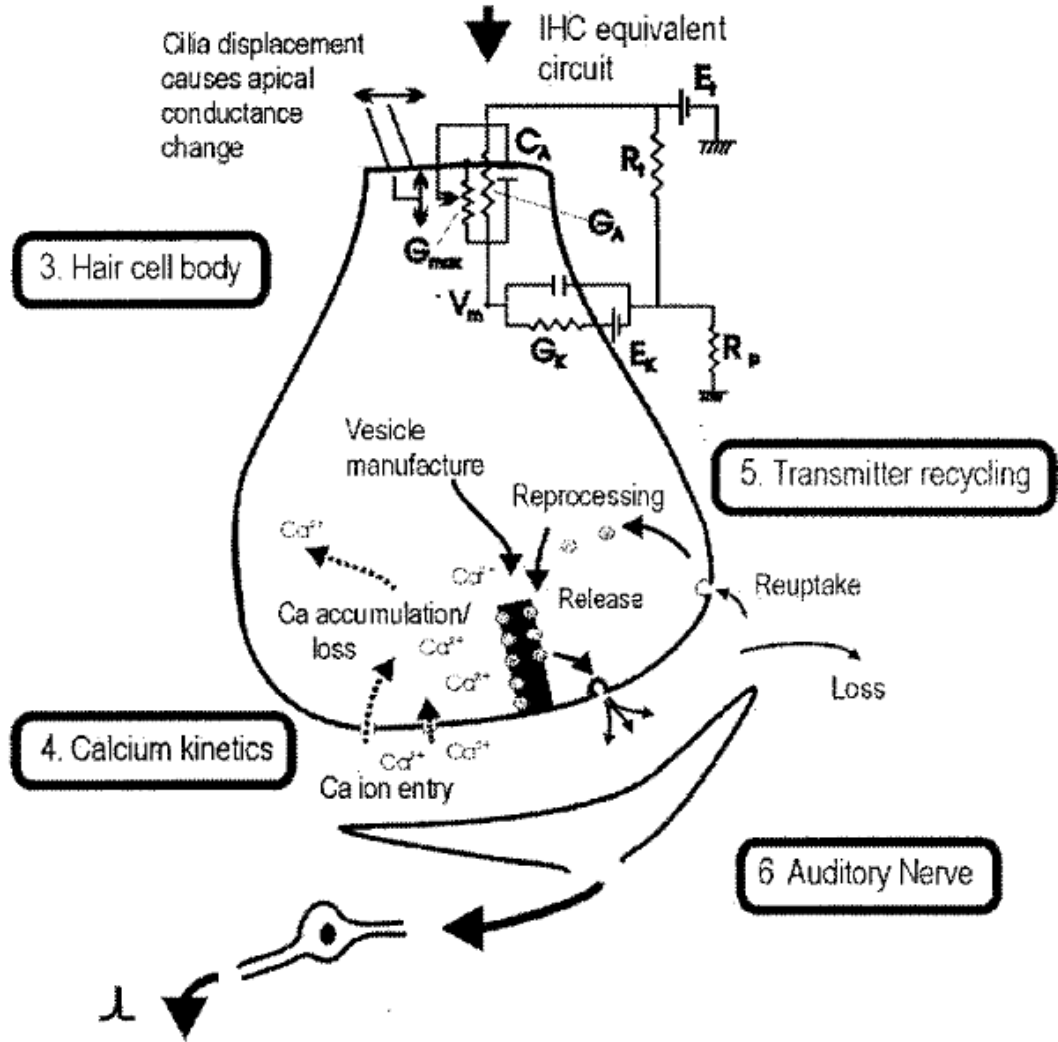


FIGURE 1.2: Basic Hodgkin-Huxley Model [3]

1.2.5 Hewitt et al. Model [4] - T-Multipolar Cell

Hewitt et al. model [4] is comprised of cell dendrite and soma models. Lu [10] used the AN output of Meddis et al. model as the input of Hewitt et al. model, and obtained the outputs of TM cells.

1.2.6 Thesis Organization

The thesis has 5 chapters, first we will introduce the basic knowledge of hearing system, then the reference works, and finally the proposed models.

1. Chapter 1 - Introduction

Giving a brief introduction to the contents and structure of this thesis.

2. Chapter 2 - Peripheral auditory system

Introducing the peripheral auditory system, including the outer ear, the middle ear, and the inner ear. The inner ear contains the organ of Corti, and the residing inner hair cells and outer hair cells. Some of the reference models are introduced: Liu and Neely Model, Sumner et al. Model, and Hewitt et al. Model.

3. Chapter 3 - Higher auditory Pathway

Introducing the masking effect, anti-masking effect, the inhibitory interneuron, and tuberculoventral cell in the dorsal cochlear nucleus. Then, presenting the new MOC and TUB models based on the anti-masking effect. The computer-based experiments are conducted, then the data are collected and analyzed.

4. Chapter 4 - Conclusion

The conclusion and future works are summarized.

Chapter 2

Peripheral Auditory System

The mammalian auditory system consists of sensory organs (peripheral auditory system) and the central auditory system. The peripheral auditory system starts with the ear, and ends with auditory nerves. This part performs mechano-electrical transduction, which converts sound pressure waves into neural action potentials. The other part, the central auditory system, ranges from the auditory brainstem to the auditory cortex. It transmits nervous information to the brain.

According to the transmitting direction, the auditory pathway can be divided into the ascending pathway and the descending pathway. The ascending pathway is mainly for collecting sensory information, and the descending pathway is mainly for mediating the responses to acoustical stimuli.

2.1 Outer Ear

The outer ear (Figure 2.1 left part) consists of the pinna and the ear canal (external auditory meatus). The pinna captures the sounds, amplifies them, and directs them into the middle ear through the ear canal.

In the Liu and Neely model, the stimulus sound produced by a diaphragm is delivered directly through a coupler into the eardrum. The functions of the outer ear is neglected in this model. The dynamics of diaphragm can be described as

$$M_d \ddot{v}_d = f(t) - R_d \dot{v}_d - K_d x_d - P_d A_d, \quad (2.1)$$

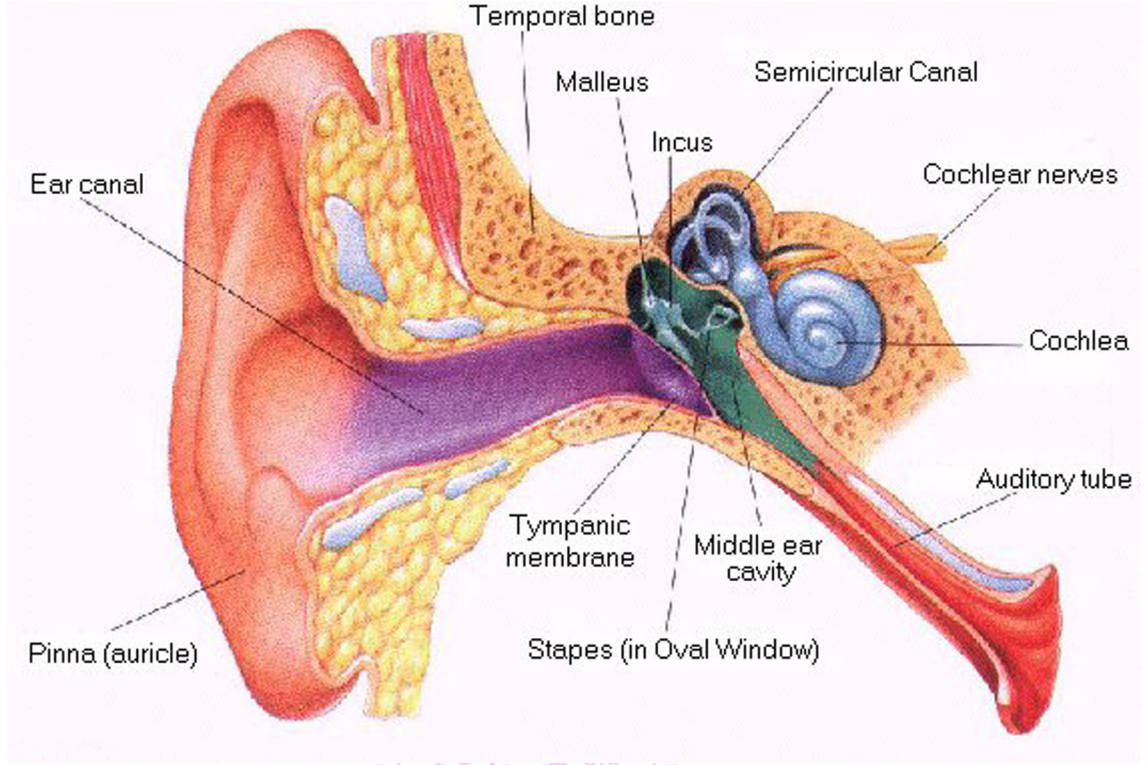


FIGURE 2.1: Anatomy of the Human Ear¹

where $f(t)$ is the force acted on the diaphragm, v_d and x_d represent the velocity and the displacement of the diaphragm, and P_d denotes the acoustic pressure in the enclosed space between the diaphragm and the eardrum. After this sound coupling mechanism, the acoustic input pressure, P_{ED} , at the eardrum is obtained.

There are two assumptions: the coupler is acoustically lossless, and the dimension of the coupler is much smaller than the stimulus wave lengths. Consequently, P_d is nearly equal to P_{ED} .

2.2 Middle Ear

The middle ear (Figure 2.1 middle chamber) connects the outer ear and the inner ear, starting from the tympanic membrane (eardrum) and ending at the oval window. The middle ear contains three ossicles: the malleus, the incus, and the stapes. The malleus attaches to the eardrum, and the stapes attaches to the oval window. The main function

¹<http://best-diving.org/specific-diving-diseases/172-diving-ear-anatomy-and-physiology-external-middle-and-inner-ear?start=1>

of the middle ear is to convert the compression waves in the air to fluid–membrane waves within the cochlea. First, the sound comes to the ear canal and vibrates the eardrum, it thus pushes the malleus. After the leverage of ossicles, the stapes hits the oval window and generates the fluid–membrane waves.

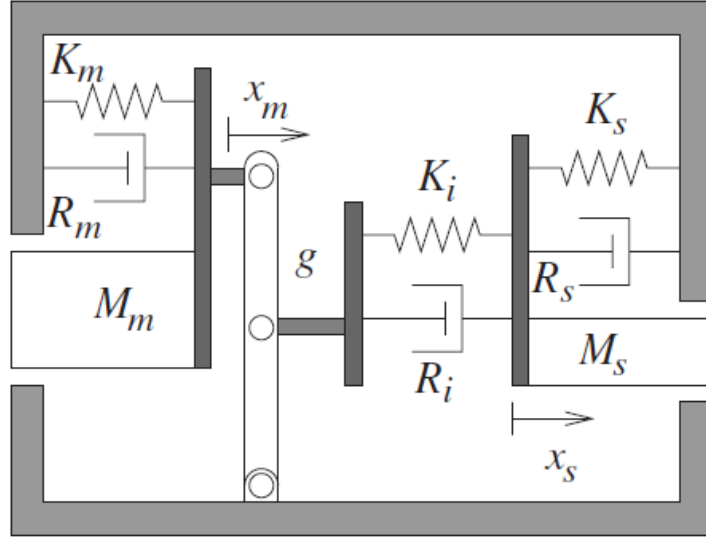


FIGURE 2.2: Matthews' Middle Ear Model [2]

The middle ear model is adapted from the model proposed by Matthews [14]. This model focuses on the mechanics of the ossicular chain, and uses mechanical components to build up a linear system. The schematic diagram is showed on Figure 2.2 [2], and the equations are shown as followings:

$$M_m \dot{v}_m = -K_m x_m - R_m v_m + g f_i + P_{ED} A_e, \quad (2.2)$$

$$(M_s + M_r) \dot{v}_s = -(K_s + K_r) x_s - (R_s + R_r) v_s - f_i - P_{FL} A_s, \quad (2.3)$$

$$f_i = K_i (x_s - g x_m) + R_i (v_s - g v_m), \quad (2.4)$$

where P_{ED} and P_{FL} are the middle ear input and output, and represent acoustic pressure at the eardrum and the fluid pressure in the vestibule, respectively. A_e and A_s are effective areas of the eardrum and the stapes footplate. The malleus is characterized by $\{K_m, R_m, M_m\}$. The incudo-stapedial joint (ISJ) is characterized by $\{K_i, R_i\}$, and the force, f_i , transferred through the ISJ is described in (2.4). The stapes is characterized by $\{K_s, R_s, M_s\}$. The round window is characterized by $\{K_r, R_r, M_r\}$. The malleus-incus leverage ratio is represented by g ($g \leq 1$).

2.3 Inner Ear

The inner ear consists of two main functional parts: the cochlea, devoted to hearing, and the vestibular system, dedicated to balance. This research is focused on the hearing system, so the vestibular system is omitted.

2.3.1 Cochlear System

In the cochlea, the fluid-membrane waves are transformed into electrical impulses, which is then sent to the central auditory system.

As Figure 2.1 shows, the cochlea resembles a snail shell. The cochlea is a spiral tube usually with 2 to 4 turns. Figure 2.3 [6] A shows a cross section through the cochlea, in which case the cochlea has about 3 turns. Figure 2.3 [6] B shows the cross section of cochlear duct. The cochlear duct consists of three chambers which are filled with fluid: the scala vestibuli, the scala media, and the scala tympani. These chambers are separated by Reissner's membrane and the basilar membrane (BM) as Figure 2.3 [6] B shows. The scala vestibuli and the scala tympani are filled with perilymph, which has higher concentration of sodium and lower concentration of potassium. The scala media is filled with endolymph, which has higher concentration of potassium and lower concentration of sodium. The different ionic composition of perilymph and endolymph causes electrochemical gradient, which drives different ionic current through various ionic channels in hair cells. This mechanism plays an important role in the inner ear organs [17].

On the BM, there sits the organ of Corti. And there are many important auditory sensory cells, hair cells in it. The hair cell can be categorized into the outer hair cell (OHC) and the inner hair cell (IHC). In the organ of Corti, there are about 3500 IHCs and 14000 OHCs.

While the membrane-fluid pressure is transduced in to the cochlea, it travels along the cochlear duct and causes pressure differences in different positions. Liu and Neely model assumes that the mechanism follows the continuum mechanics, then the membrane-pressure brings the basilar membrane to vibrate accordingly.

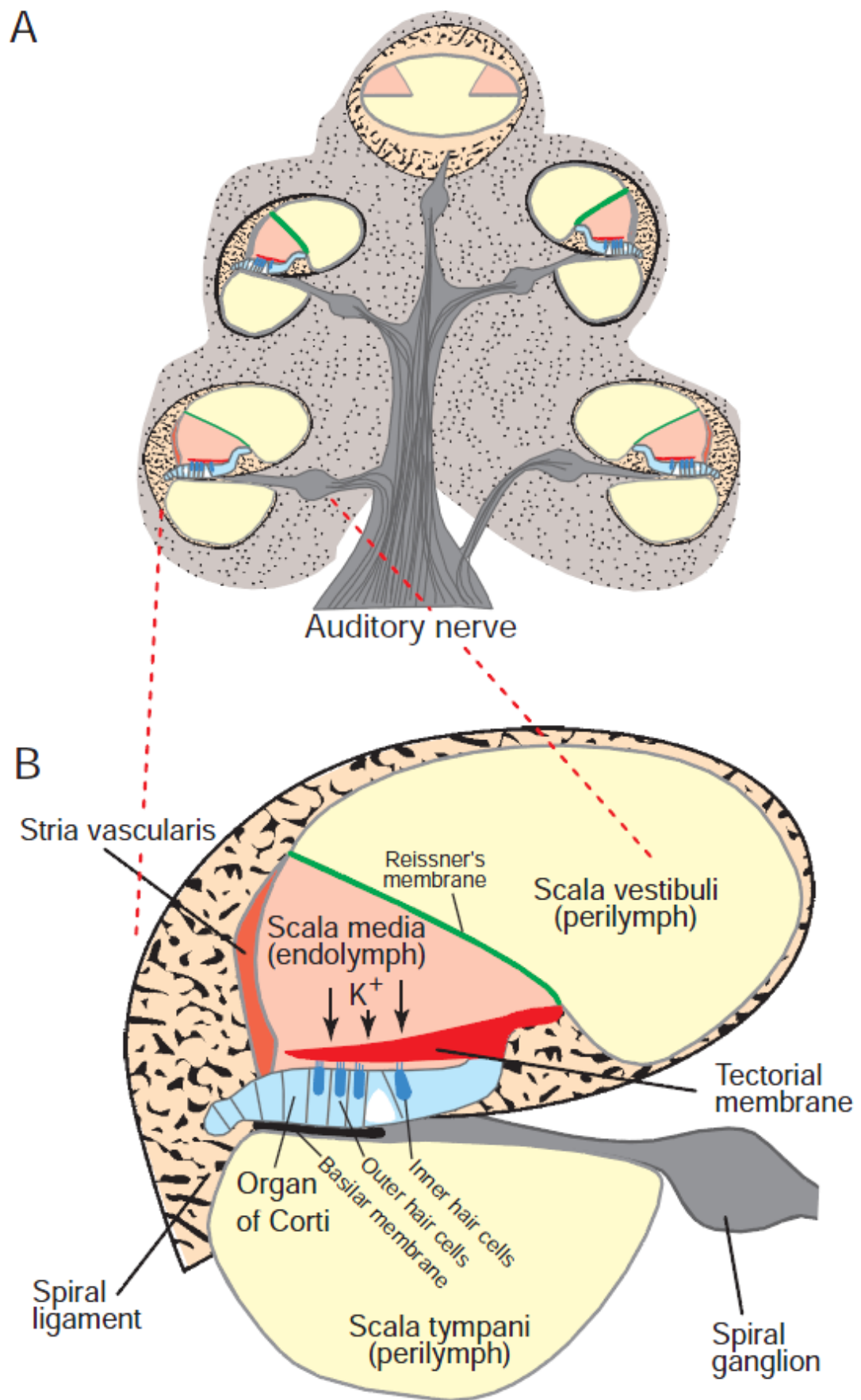


FIGURE 2.3: Cross Section through (A) the Cochlea, and (B) One Cochlear Turn [6]

First, the Newton's second law governs that

$$\partial_x P = -\frac{\rho}{A} \dot{U}, \quad (2.5)$$

where P denotes the pressure difference between scala vestibuli and scala tympani, x denotes the direction of cochlear duct from base to apex, ρ denotes the effective fluid mass density, A denotes the cross-sectional area, and U denotes the volume velocity along the x -direction. And there are two boundary conditions at the basal end (oval window and round window)

$$\partial_x P|_{x=0} = -\rho \dot{v}_s, \quad (2.6)$$

where v_s denotes the velocity of the stapes, and the apical end

$$\partial_x P|_{x=L} = \frac{-\rho}{Am_h} P, \quad (2.7)$$

where Am_h denotes the acoustic inductance at the helicotrema. By using the principle of continuity, the following equation can be written

$$\partial_x U = w \dot{\xi}_r, \quad (2.8)$$

where w is the width of the cochlear partition.

Second, the basilar membrane is driven by the membrane-fluid pressure

$$m \ddot{\xi}_b + r \dot{\xi}_b + k \xi_b = -P, \quad (2.9)$$

$$\xi_b = \xi_r + \xi_o, \quad (2.10)$$

where ξ_b , ξ_r , ξ_o are displacement of the basilar membrane, the reticular lamina, and the outer hair cell, respectively. Also, m , r , k are mass, resistance, stiffness of BM per unit area.

2.3.2 Place Theory

The place theory states that the perception of hearing depends on the vibration position of BM (Figure 2.4 [7]). The BM is narrow and thin near the base but wide and thick near the apex. Also, BM at the base is stiffer than at the apex. The different stiffness

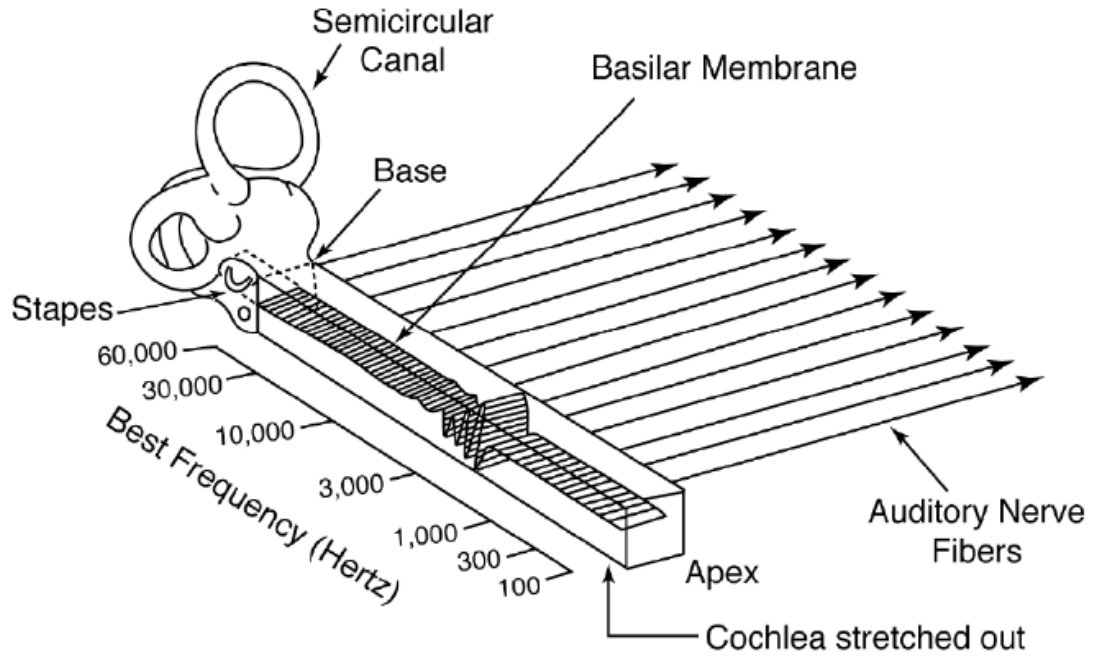


FIGURE 2.4: Place Theory [7]

at different positions of BM makes them have different characteristic frequencies (CF). According to the simple harmonic motion formula

$$f = \frac{1}{2\pi} \sqrt{\frac{k}{m}}, \quad (2.11)$$

where f is equivalent to the CF, k is equivalent to the stiffness, and m is equivalent to the BM mass per unit area. Therefore, the CFs of the BM from the base to the apex distribute from high to low. The distribution of CF along BM is called tonotopy or tonotopic mapping.

In the Liu and Neely model, the parameters of cochlea are divided into three parts: the base, the mid, and the apex. Each part has different physical properties. For example, the mass, the resistance, and the stiffness per unit area of the BM are distinct in different parts. The parameters of the remaining segments are then obtained by using interpolation, so they distribute from low to high or from high to low in a continuous fashion.

2.3.3 Outer Hair Cell

OHCs are believed to amplify the traveling waves along the BM. OHCs contract or stretch their cell body if they are stimulated electrically. The mechanical response is voltage dependent. Depolarizing stimuli causes it to contract, and hyperpolarizing stimuli causes it to stretch. By changing OHCs' length in a cycle-by-cycle basis, they amplify the waves traveling along the BM.

2.3.4 OHC Mechanoelectrical Transduction

The vibration of BM causes the hair bundle (HB) on the OHC to deflect, thus the current flowing into the cell body changes, and the OHC is depolarized or hyperpolarized.

The receptor current i_r is modeled as the nonlinear equation

$$i_r = I(\eta) = \frac{I_{\max}}{2} \tanh \frac{2\eta}{I_{\max}}, \quad (2.12)$$

where

$$\eta = \alpha_v \dot{\xi}_r + \alpha_d \xi_r. \quad (2.13)$$

2.3.5 OHC Electromotility

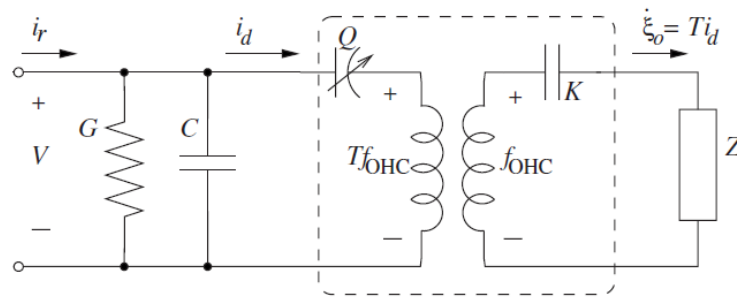


FIGURE 2.5: OHC Model [1]

The OHC model is constructed by using electric components as Figure 2.5 [1] shows. The capacitance and conductance of plasmic membrane are modeled as C and G , and the gating charge is represented by Q . There is also a pizeoelectrical component $T f_{OHC}$, which converts the contracting force, f_{OHC} , into the electrical potential difference.

By using Kirchhoff's current law (KCL), the equation can be written as

$$i_r = C \frac{dV}{dt} + GV + C_g \frac{d\tilde{V}}{dt}, \quad (2.14)$$

where

$$\tilde{V} = V - T f_{OHC}. \quad (2.15)$$

Second, the contracting force is generated by the contraction and stretch of the OHC.

The OHC contraction displacement, ξ_o , is assumed to be linearly proportional to Q ,

$$\xi_o = TQ, \quad (2.16)$$

and the contraction/stretch generates the contracting force,

$$f_{OHC} = M\ddot{\xi}_o + R\dot{\xi}_o + K\xi_o, \quad (2.17)$$

2.3.6 State-space Formulation

The state-space equations are listed, so the change amount can be directly calculated by giving the following state variables.

$$\dot{\xi}_r = u_r, \quad (2.18)$$

$$\dot{Q}(x) = T^{-1}u_o, \quad (2.19)$$

$$\dot{u}_r(x) = \frac{Ru_o + KTQ}{M} - \frac{V - C_g^{-1}Q}{TM} - \frac{r(u_r + u_o) + k(\xi_r + TQ)}{m} - \frac{P(x)}{m}, \quad (2.20)$$

$$\dot{u}_o(x) = -\frac{Ru_o + KTQ}{M} + \frac{V - C_g^{-1}Q}{TM}, \quad (2.21)$$

$$\dot{V}(x) = \frac{1}{C}(i_r(u_r, \xi_r) - GV - T^{-1}u_o). \quad (2.22)$$

The detailed derivation of Eq. (2.18) to (2.22) are described in Appendix B. The variable $P(x)$ in (2.20) can be calculated by using

$$\left(\partial_x^2 - \frac{\rho w}{mA}\right)P = l(u_r(x), u_o(x), \xi_r(x), Q(x), V(x)), \quad (2.23)$$

which is the combination of (2.7) and (2.8),

$$\partial_x^2 P = -\frac{\rho}{A} \left(\partial_x \partial_t U - \partial_t U \frac{\partial_x A}{A} \right) \quad (2.24)$$

$$\approx -\frac{\rho}{A} w \partial_t^2 \xi_r. \quad (2.25)$$

The last term in (2.25) is ignored by supposing the area change in x -direction, $\partial_x A$, is small compared to the entire cross-sectional area, A .

2.3.7 Inner Hair Cell

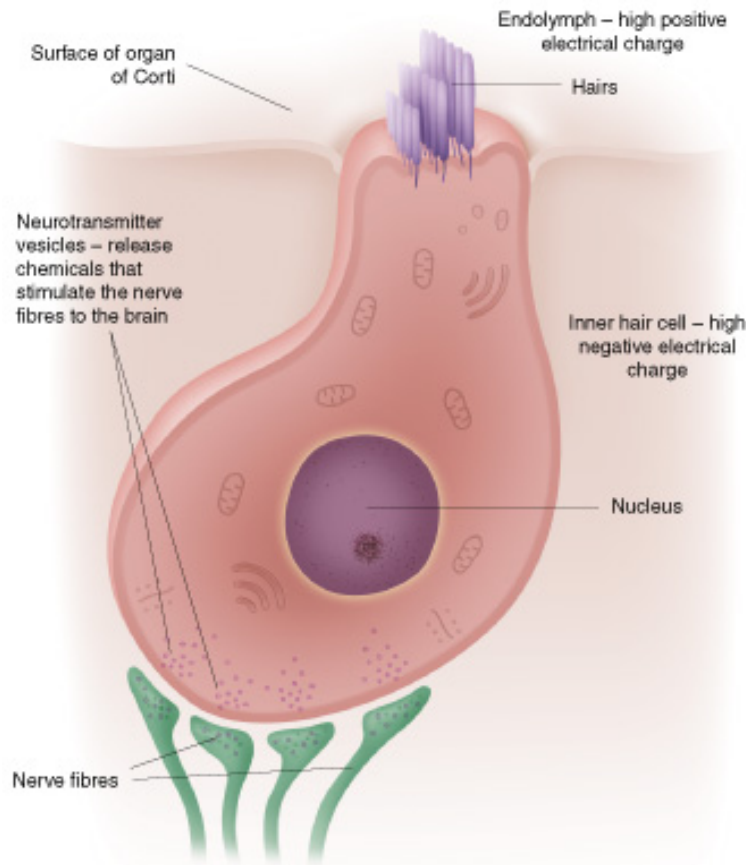


FIGURE 2.6: Inner Hair Cell²

The primary function of IHC is to transduce BM motion into neural signals. When the waves travel along the BM, the hair cells, which are attached on the organ of Corti, are brought to make shearing movement. The stereocilia (Figure 2.6), which are attached on the top of the hair cell body, then are deflected and the opening rate of tension triggered

²http://www.hearingaidscentral.com/How-the-human-ear-works_ep_51.html

transducer channels is increased or decreased according to the deflection direction. If the stereocilia deflect to the direction of the tallest one, the hair cells are depolarized. If the stereocilia deflect to the opposite direction, the hair cell is hyperpolarized.

2.3.8 IHC Model

The IHC model is referred to Sumner et al.'s work [3], which assembles the different functions of the IHC. The IHC model is mainly comprised of three parts: cilia displacement causing conductance change then the intracellular potential change, the calcium kinetics dominated by the receptor potential, and the quantal and probabilistic model of vesicles of neurotransmitter.

2.3.8.1 IHC Receptor Potential

According to Shamma et al.'s previous work [18], the relationship between IHC cilia and BM is

$$\tau_c \frac{du(t)}{dt} + u(t) = \tau_c C_{\text{cilia}} v(t), \quad (2.26)$$

where $u(t)$ is the displacement of the IHC cilia, $v(t)$ is the BM velocity, C_{cilia} is a gain factor and τ_c is a time constant. In the light of this equation, the cilia moves with BM velocity at low frequency and with BM displacement at high frequency. This can be proved by taking Fourier transform of (2.26).

After the BM motion is transduced to the IHC cilia, the ion channels are open, and then the apical conductance, $G(u)$ changes. In accordance with Mountain and Hubbard's work [19], the relation between $u(t)$ and $G(u)$ is

$$G(u) = \frac{G_{\text{cilia}}^{\max}}{1 + \exp\left(-\frac{u(t)-u_0}{s_0}\right) \left[1 + \exp\left(-\frac{u(t)-u_1}{s_1}\right)\right]} + G_a, \quad (2.27)$$

where G_{cilia}^{\max} is the transduction conductance when all ion channels open, G_a is the passive conductance. u_0 , s_0 , u_1 , s_1 are constants which shape the nonlinearity of the conductance.

Based on Shamma et al.'s model [18], the membrane potential is modeled in electrical circuit as Figure 2.7 [18] shows. By using Kirchhoff's current law (KCL), the following

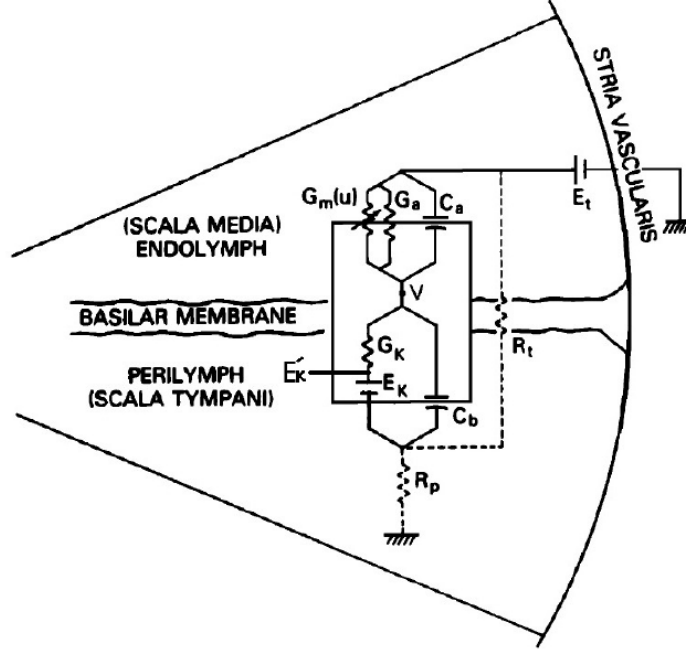


FIGURE 2.7: IHC Membrane Potential Model [18]

equation can be written

$$(C_a + C_b) \frac{dV(t)}{dt} + [G_m(u(t)) + G_a] (V(t) - E_t) + G_k(V(t) - E'_k) = 0, \quad (2.28)$$

where $V(t)$ is the intracellular hair cell potential; C_a is the capacitance on the apex; C_b is the capacitance on the base; $G_m(u(t))$ is the left term of (2.27); G_a is the right term of (2.27); G_k is the voltage-invariant basolateral membrane conductance; E'_k is

$$E'_k = E_k + \frac{E_t R_t}{R_t + R_p}, \quad (2.29)$$

where R_t and R_p are the resistance of the supporting cells. Then, (2.28) can be simplified to

$$C_m \frac{dV(t)}{dt} + G(u)(V(t) - E_t) + G_k(V(t) - E'_k) = 0, \quad (2.30)$$

by assuming

$$C_m = C_a + C_b, \quad (2.31)$$

and

$$G(u) = G_m(u(t)) + G_a. \quad (2.32)$$

Finally, we obtained the IHC receptor potential (RP), $V(t)$, by delivering the BM velocity, $v(t)$, to this IHC receptor potential model.

2.3.8.2 Calcium Controlled Transmitter Release Function

After the IHC is depolarized, the calcium ion channels are open and produce a calcium current. Sumner et al. adapted Hudspeth and Lewis [20] and Kidd and Weiss [21]'s work, and change the time constant to be independent of voltage. The calcium current, $I_{Ca}(t)$, changes with $V(t)$ in the following manner,

$$I_{Ca}(t) = G_{Ca}^{\max} m_{I_{Ca}}^3(t)(V(t) - E_{Ca}), \quad (2.33)$$

where E_{Ca} is the reversal potential, G_{Ca}^{\max} is the conductance in the synapse when all calcium channels open. $m_{I_{Ca}}$ is the fraction of calcium channels which are open, it is modeled as

$$\tau_{I_{Ca}} \frac{dm_{I_{Ca}}(t)}{dt} + m_{I_{Ca}}(t) = m_{I_{Ca},\infty} \quad (2.34)$$

where $\tau_{I_{Ca}}$ is a time constance. $m_{I_{Ca},\infty}$ is the steady-state value of $m_{I_{Ca}}(t)$, and is controlled by $V(t)$

$$m_{I_{Ca},\infty} = \frac{1}{1 + \frac{1}{\beta_{Ca}} e^{-\gamma_{Ca} V(t)}} \quad (2.35)$$

After the calcium current flow into the cell, some calcium ions are accumulated in the vicinity of the synapse. According to Hudspeth and Lewis[20], the first-order, low-pass-filter equation of calcium concentration, $[Ca^{2+}]$, is modeled as

$$\tau_{[Ca]} \frac{d[Ca^{2+}](t)}{dt} + [Ca^{2+}](t) = I_{Ca}(t), \quad (2.36)$$

where $\tau_{[Ca]}$ is a time constant.

In accordance to Augustine et al [22], the calcium concentration is proportional to transmitter release rate, $k(t)$. Based on their experiment data, Sumner et al. deployed the transmitter release rate function

$$k(t) = \max([Ca^{2+}]^3(t) - [Ca^{2+}]_{thr}^3, 0), \quad (2.37)$$

where $[Ca^{2+}]_{thr}^3$ is a threshold constance, and z is a scalar factor.

2.3.8.3 Quantal and Probabilistic Model of Synaptic Adaptation

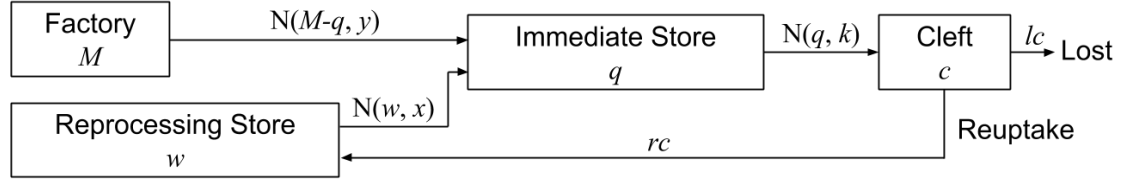


FIGURE 2.8: Meddis Model

Once the IHC is depolarized, it releases transmitters to AN. Sumner adapted Meddis [16]’s non-quantal transmitter model to the quantal and stochastic model.

$$q(t + \Delta t) - q(t) = N(w(t), x) + N([M - q(t)], y) - N(q(t), k(t)), \quad (2.38)$$

$$c(t + \Delta t) - c(t) = N(q(t), k(t)) - lc(t) - rc(t), \quad (2.39)$$

$$w(t + \Delta t) - w(t) = rc(t) - N(w(t), x). \quad (2.40)$$

These equations can be analyzed as shown in Figure 2.8. M , q , C are non-negative integers, which represent the number of vesicles; w is a decimal number, which represents the amount of neuron transmitter. Equation (2.38) describes the changes of vesicles at the immediate store. The total number change of vesicles at immediate store, q , in a duration, Δt , is the number from factory, which produce $N(M - q, y)$ vesicles, adding the reprocessed $N(w, x)$ vesicles, subtracting the $N(q, k)$ transmitted vesicles. Equation (2.39) describes the changes of vesicles at the cleft. The total vesicle change is $N(q, k)$ transmitted from immediate store, subtracting lc transmitter loss, and subtracting rc reuptake transmitter. The vesicles at the cleft release the transmitter, which is represented by decimal numbers; one vesicle at the cleft releases one transmitter, and one transmitter at reprocessing store forms one vesicle. Equation (2.40) describes the transmitter change at reprocessing store. The total change is those from cleft subtracting those are reproduced to vesicles and released to the immediate store. $N(n, \rho)$ is a quantal and stochastic function representing how many of the n vesicles are released, and each vesicle has the same probability, $\rho\Delta t$, to be released.

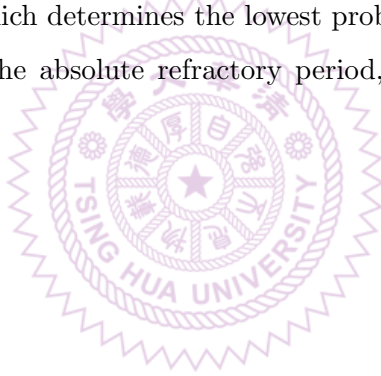
2.3.9 Auditory Nerve

The auditory nerve (AN), also known as cochlear nerve, transmits sound signals from the IHC to the brain. The dendrites receive signals from the IHC, and the axon innervates to the cochlear nucleus (CN).

Siegel [23] suggested that a vesicle of transmitter released at the dendrites is sufficient to activate an action potential (AP) in an experiment conducted on guinea-pigs. Sumner et al. use this result to build an AN model. When at least a vesicle is released to the cleft, the probability, $P(t)$, to produce an AP is

$$P(t) = \begin{cases} 0, & \text{for } (t - t_l) < R_A \\ 1 - c_r e^{-\frac{t - t_l - R_A}{s_r}}, & \text{for } (t - t_l) \geq R_A, \end{cases} \quad (2.41)$$

where c_r is a constant which determines the lowest probability $1 - c_r$ when the relative time $t - t_l$ is just over the absolute refractory period, R_A , and t_l is the time of the previous AP.



Chapter 3

Higher Auditory Pathway

This chapter includes part of the central auditory system, the cochlear nucleus (CN), and a descending pathway, the medial olivocochlear (MOC) reflex. First, the masking effect can be simulated by simply designing a proper stimulus input. Then, the MOC model is constructed to simulate the anti-masking effect in tone-burst-in-noise condition. The CN have many kinds of interneurons, and complex excitatory and inhibitory mechanics. We use the T-multipolar (TM) cells, which are located in the ventral cochlear nucleus (VCN), model constructed by Hewitt et al. [4] as the interneuron between the auditory nerve (AN) and the MOC. Finally, the TUB cells, which are located in the deep layer of dorsal cochlear nucleus (DCN), model is proposed to inhibit the TM cells. We also propose the lateral inhibition model of TUB cells to inhibit the neighbor TUB cells. By combining these two negative feedbacks, the anti-masking effect is enhanced in sustained-tone-in-noise condition.

3.1 Masking Effects

Masking effects occur when perception of a target sound is affected by presence of other sounds. There are two categories of masking: frequency-domain masking and time-domain masking. The former happens when the masker appears with target signal simultaneously. The latter happens when the masker appears before or after the target signal.

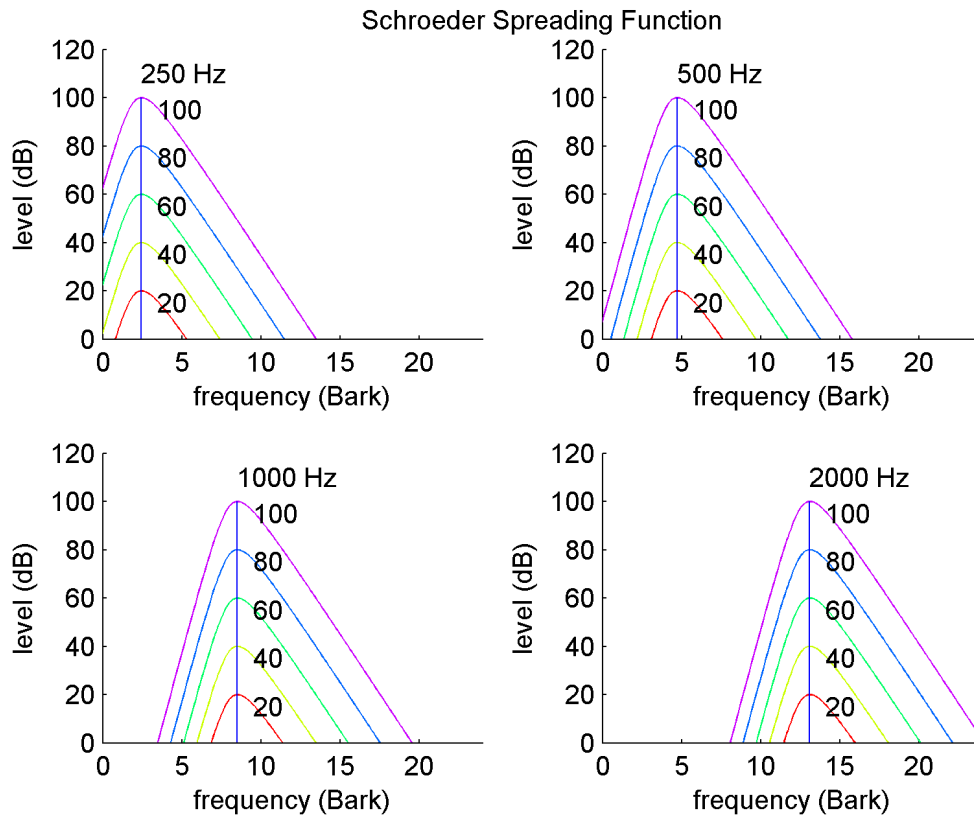


FIGURE 3.1: Masking Audiograms

Two-tone masking is shown on audiograms (Figure 3.1) by using Schroeder spreading function[24]. The straight vertical line in each audiogram represents masker, and its frequency is labeled on top of it. Each audiogram has 5 intensities of masker (20, 40, 60, 80, 100 dB), and each intensity corresponds to a threshold curve. The target signal has to exceed the threshold to be perceived by human.

Wide-band and narrow-band noise maskers are more complicated, but have been well studied [25]. They are better maskers than a pure tone one; that is, the threshold of the pure tone is lower to be perceived.

The masking effect plays an important role in our daily life. For example, on a quiet street, two people are chatting. When a noisy truck passes by, their conversation will be interrupted. There are two options to overcome this condition. First, they can wait until the truck to leave, that is to remove the masker. Second, they can raise their voice, that is to raise the maskee level. However, masking effect is not always negative. With

the masking effect, we are able to concentrate on the target sound rather than hearing trivial noise.

3.1.1 Model Structure

The reference models are formed by Liu and Neely's model from middle ear to BM, Sumner et al's model from BM to AN, and Hewitt et al's TM neuron model as Lu previously constructed (Figure 3.2). Then, a new proposed MOC and TUB model is connected to the outputs of TM and AN respectively. Liu and Neely's model is quantized to 700 points along the tonotopic map representing 700 segments with equal length. Sumner et al, Hewitt et al's, and proposed models are downsampled into 70 points (Figure 3.3). Based on these series of models, the input stimulus is designed and the output signals are collected from AN. Finally, we analyze the statistics of the results.

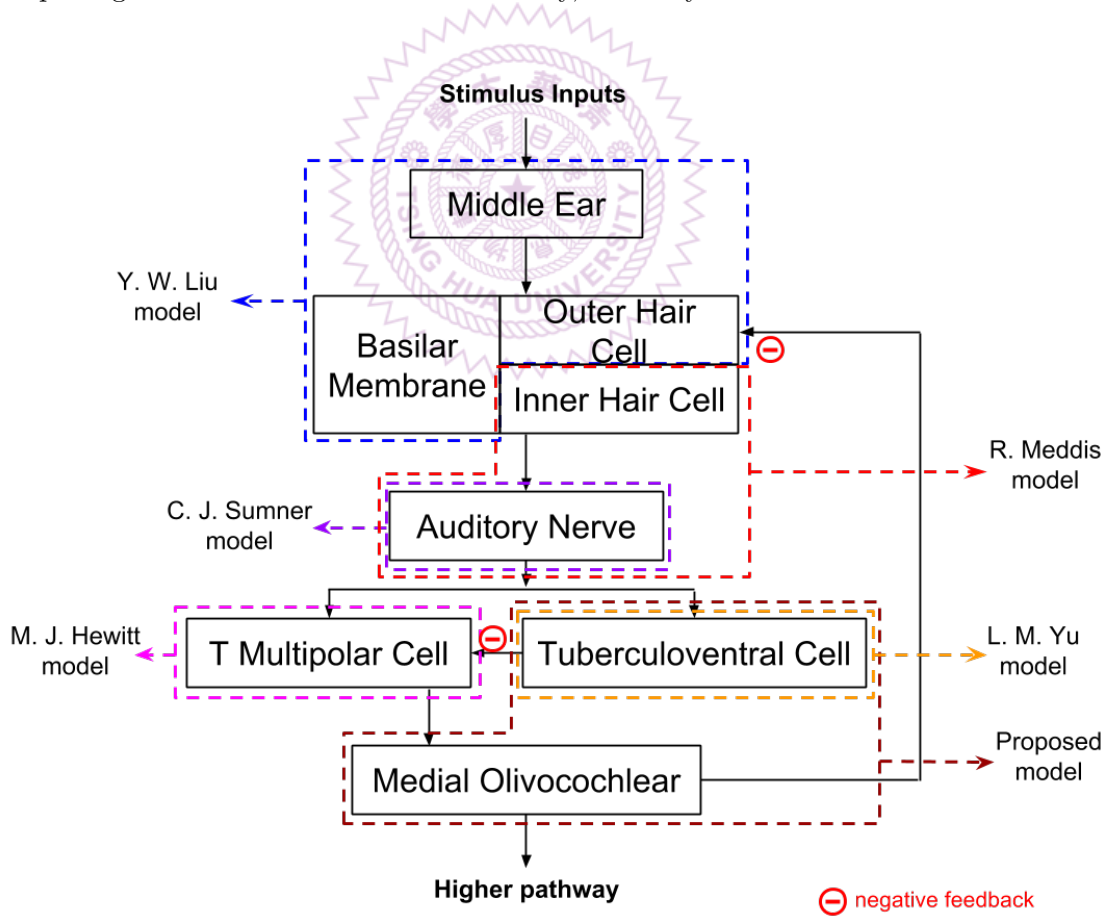


FIGURE 3.2: Model Diagram

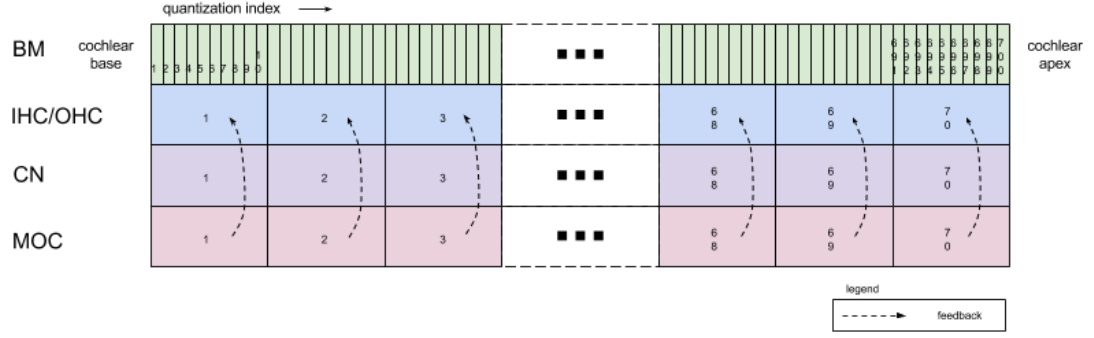


FIGURE 3.3: Spatial Quantization Index

3.1.2 Simulation Setup

To simulate the masking effect, the stimulus sound is constructed as tone bursts in sustained noise, and the TM, TUB, and MOC models are not yet included. The noise is a 37 dB SPL and 400 ms long white noise. The tone burst is a 4000 Hz, 100 ms long sinusoidal signal which begins at $t = 300$ ms and ends at $t = 400$ ms, relative to the noise. A complete stimulus repeats and concatenates the above settings 3 times, so the total length is 1200 ms. For the purpose of rate-level (RL) plots, the tone level is swept from 0 to 100 dB SPL, and the simulation is repeated 5 times. Consequently, there are 15 simulation results, which then are used for statistics. Figure 3.4 is an example of tone burst in noise stimulus with 50 dB tone level. The top panel is a 37 dB sustained white noise. The middle panel are three 50 dB tone burst, and each is 100 ms long. The bottom panel is the final stimulus which is the sum of the tone and the noise.

3.1.3 Experiment Result

Figure 3.5 shows the simulation results. The blue one indicates the RL plot of AN of masking effect. The solid curve represents the mean of 15 times results, the dashed lines with ranges represents the standard errors at specific RL. The RL curve demonstrates that when the tone level increases, the discharge rate of AN also increases. However, due to the masking effect, it compresses the dynamic range of AN. This will make it difficult for human ear to distinguish tones between different levels. Nevertheless, thanks to the anti-masking effect, which will be showed in the next section, the dynamic range is broadened.

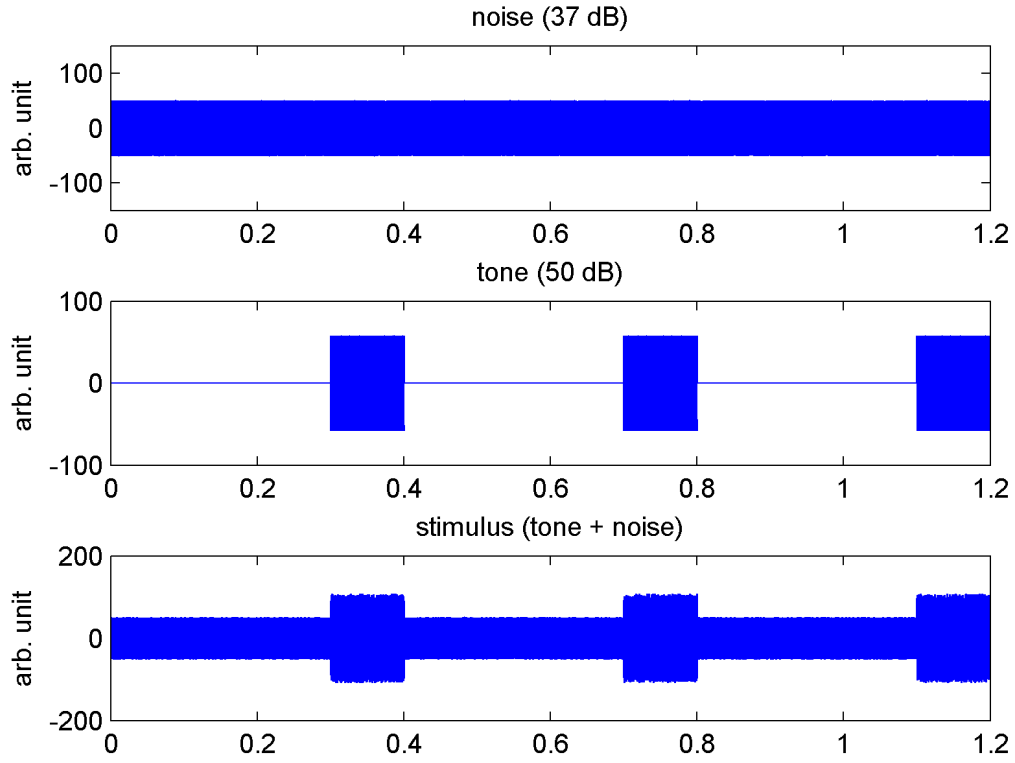


FIGURE 3.4: Stimulus

3.2 Cochlear Nucleus

The cochlear nucleus (CN) is located at the dorso-lateral side of the mammalian brainstem and receives auditory inputs from the cochlear nerve. The outputs of CN are projected to higher regions of the auditory brainstem. Each CN can be divided into two regions: dorsal cochlear nucleus (DCN) and ventral cochlear nucleus (VCN).

The TM cell is one of the interneurons of VCN. We use TM cells to transmit neural signal from ANs to the MOC. The TM cell model is adopted from Hewitt et al[4]. This model is comprised of the cell dendrite and the soma models. Lu used the AN output of Meddis et al. model as the input of Hewitt et al. Model, and obtained the outputs of the TM cells.

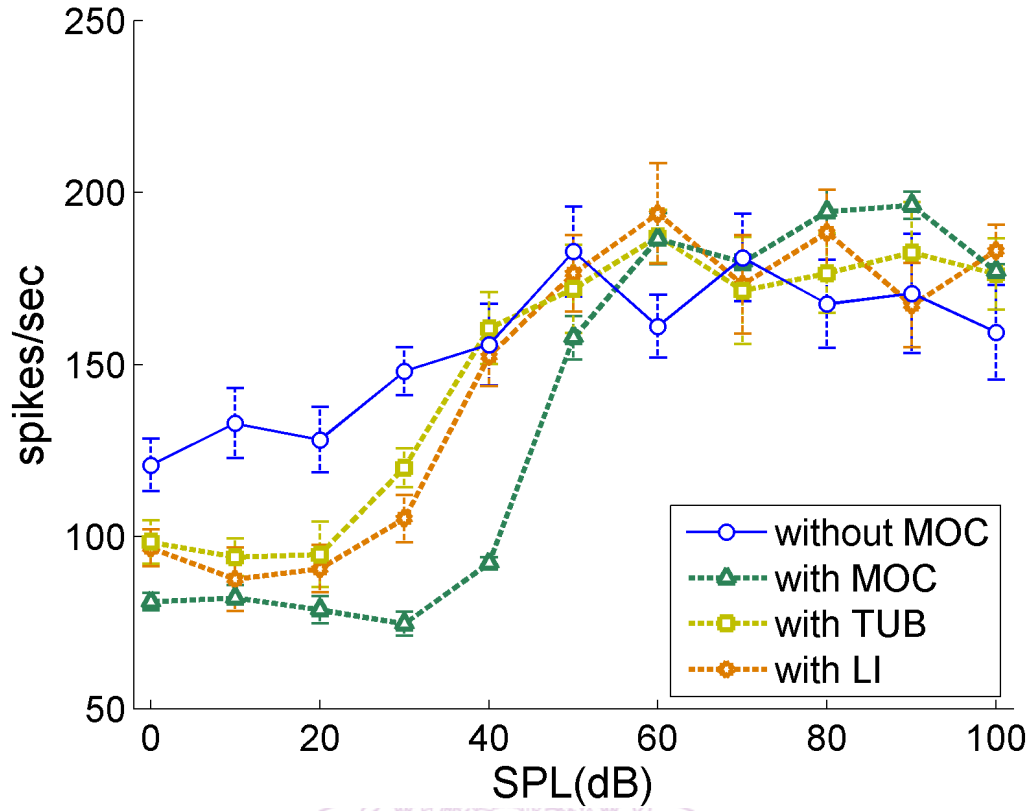


FIGURE 3.5: RL Plot of AN at Tone Burst in Noise condition

3.2.1 Dendrite Model

Most of the AN fibers converge to the dendrites of a TM cell, and only few of them directly connect to the soma[26][27]. Therefore, in the dendrite model, Hewitt applied linear summation of all dendrite inputs from ANs

$$I_d(t) = n(t)\Delta I, \quad (3.1)$$

where $I_d(t)$ is the current through the dendrite, $n(t)$ is the number of firing ANs connected to the dendrites of the TM, and ΔI is the current amount provided by a AN fiber. ΔI can be calculated as

$$\Delta I = \frac{I_{\max}}{N}, \quad (3.2)$$

where I_{\max} is the maximum current can be delivered the the soma, and N is the total number of AN fibers.

Because of the conducting media of dendrites, the current on them will be attenuated and low-pass filtered according to the cable theory[28]. Hewitt et al. use a first-order Butterworth filter, whose transfer function is

$$\frac{I_d(f)}{I_s(f)} = \frac{1}{\sqrt{1 + \left(\frac{f}{f_c}\right)^2}} \quad (3.3)$$

to simulate the low-pass effect. I_d is the dendritic current, I_s is the current flowed into the soma, and f_c is the cutoff frequency. By using the bilinear transformation method, the discrete-time filter can be obtained as following

$$I_s[n] = GI_d[n] + GI_d[n-1] - HI_s[n-1], \quad (3.4)$$

where G and H are

$$G = \frac{1}{1 + \frac{1}{\tan\left(\pi \frac{f_c}{f_s}\right)}}, \quad (3.5)$$

$$H = \frac{1 - \frac{1}{\tan\left(\pi \frac{f_c}{f_s}\right)}}{1 + \frac{1}{\tan\left(\pi \frac{f_c}{f_s}\right)}}, \quad (3.6)$$

where f_s is the sampling rate.

3.2.2 Soma Model

The soma model describes the relations between four variables, $E(t)$, $G_k(t)$, θ_{TM} , and $p(t)$. $E(t)$ is the cell-membrane potential, $G_k(t)$ is the cell potassium conductance, θ_{TM} is the firing threshold, and $p(t)$ is the output. These variables are governed by four differential equations below.

First, the transmembrane potential is characterized as

$$\frac{dE(t)}{dt} = \frac{-E(t) + \{V(t) + G_k(t)[E_k - E(t)]\}}{\tau_m} \quad (3.7)$$

$$= \frac{-E(t) + \{I_s(t)R_i + G_k(t)[E_k - E(t)]\}}{\tau_m}, \quad (3.8)$$

where R_i is the input resistance, E_k is the equilibrium potential, and τ_m is the membrane time constant.

Second, the potassium conductance is characterized as

$$\frac{dG_k(t)}{dt} = \frac{-G_k(t) + (bs)}{\tau_{Gk}}, \quad (3.9)$$

where b is the delayed rectifier potassium conductance strength, s represents that if the cell is firing (0 or 1), and τ_{Gk} is a time constant.

Third, the time-varying threshold is characterized as

$$\frac{d\theta_{TM}(t)}{dt} = \frac{-[\theta_{TM}(t) - \theta_{0,TM}] + cE(t)}{\tau_{\theta_{TM}}}, \quad (3.10)$$

where $\theta_{0,TM}$ is the resting threshold, c is a accommodation constant, and $\tau_{\theta_{TM}}$ is a time constant. s in the above section is determined by

$$s = \begin{cases} 0, & \text{if } E(t) < \theta_{TM} \\ 1, & \text{if } E(t) \geq \theta_{TM}. \end{cases} \quad (3.11)$$

Last, the all-or-nothing spiking variable is characterized as

$$p(t) = E(t) + s[E_b - E(t)], \quad (3.12)$$

where E_b is the reversal potential.

3.3 Anti-Masking Effects

Anti-masking effects appear when feedback to the auditory periphery exists. There are two major efferent feedback pathways to auditory periphery: the middle ear muscle (MEM) reflex and the olivocochlear (OC) efferent reflex (Figure 3.6 [5] and Figure 3.7 [5]). There are three major hypothesized functions of MOC:

1. To protect the ear from loud sounds [29]

2. To help to develop cochlea function [30]
 3. To enhance discrimination of sounds in noise [31]
1. and 3. are related to acoustic property of MOC reflex, and we will focus on 3. in this work.

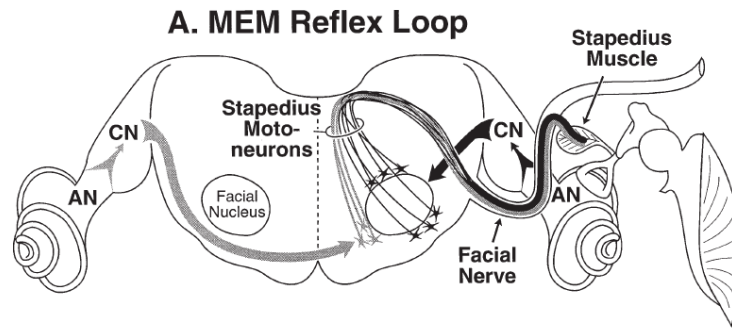


FIGURE 3.6: MEM Reflex Loop [5]

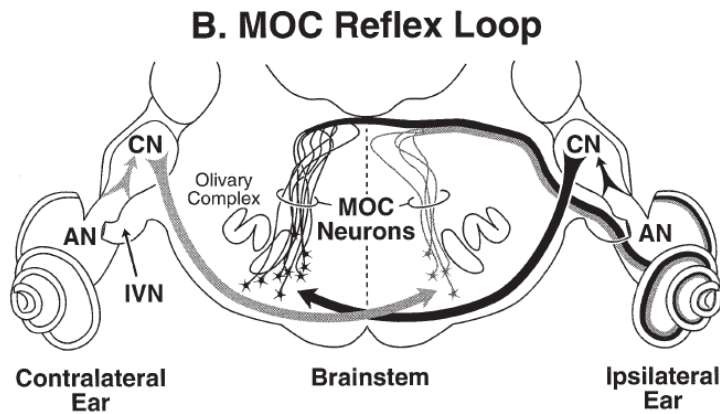


FIGURE 3.7: MOC Reflex Loops [5]

3.3.1 Experiment results of the article: Feedback Control of The Auditory Periphery: Anti-masking Effects of Middle Ear Muscles VS. Olivocochlear Efferents [5]

From Figure 3.8 [5], we can observe that both MEM and MOC attenuate a certain frequency band. MEM mainly reduces low frequency stimuli (below 2 kHz), and MOC mainly reduces mid- to high-frequency stimuli (1 to 20 kHz). Because of the mechanism of MEM and MOC, they protect our ears from damage by large sounds.

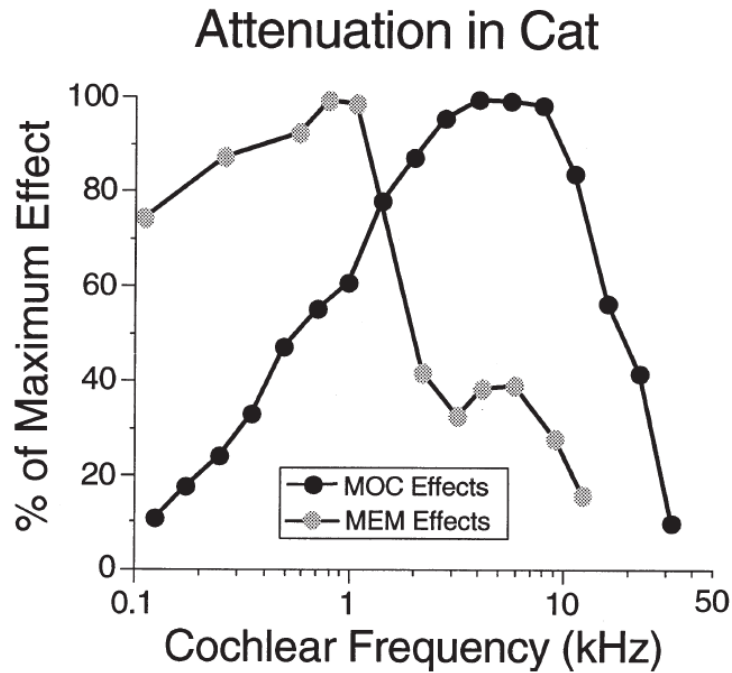


FIGURE 3.8: Comparison of the relative strength of MEM and MOC peripheral effects as a function of frequency [5]

The author introduces two masking phenomena: excitatory masking and suppressive masking. Figure 3.9 [5] shows the excitatory masking condition, when the noise is located at the same frequency band as the target sound. Because of the tonotopical organization of the cochlea, both the target signal and the noise excite the same location of the cochlea. Therefore, AN fibers keep firing, and the noise masks the target signal. Figure 3.10 [5] shows suppressive masking condition, when the noise is located at a different frequency band from the target sound. The noise elicits some frequency band of cochlear; however, the vibration of the BM at the frequency band of the noise makes it difficult for the one at the frequency band of the target sound to vibrate. Consequently, the AN fibers no longer fire, and the target signal is masked.

Between MEM and MOC reflexes, there are two different anti-masking effects (Figure 3.11 [5] and Figure 3.12 [5]). First, MEM reflex (Figure 3.11 [5]) decreases the suppressive masking effect. Figure 3.8 [5] shows that MEM reflex mainly reduces low frequency sounds. Therefore it suppresses low frequency noise, and unmask high frequency sounds. Second, MOC reflex (Figure 3.12 [5]) decreases the excitatory masking effect. Figure 3.8 [5] again shows that MOC reflex mainly reduces mid- to high-frequency sounds. Therefore, it reduces the noise interference and unmask low frequency sounds and

A. Excitatory Masking

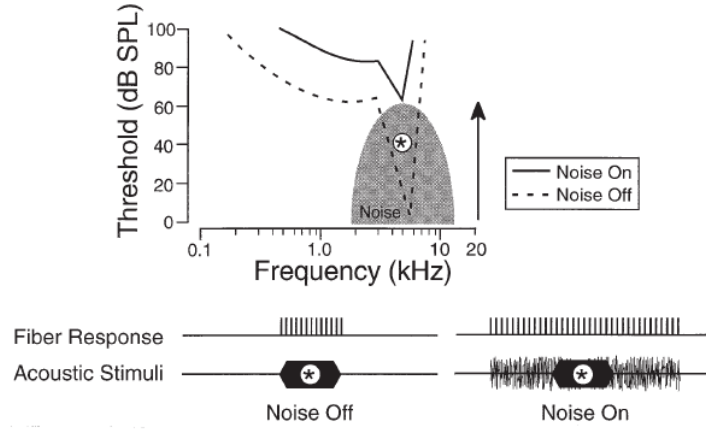


FIGURE 3.9: Excitatory Masking [5]

B. Suppressive Masking

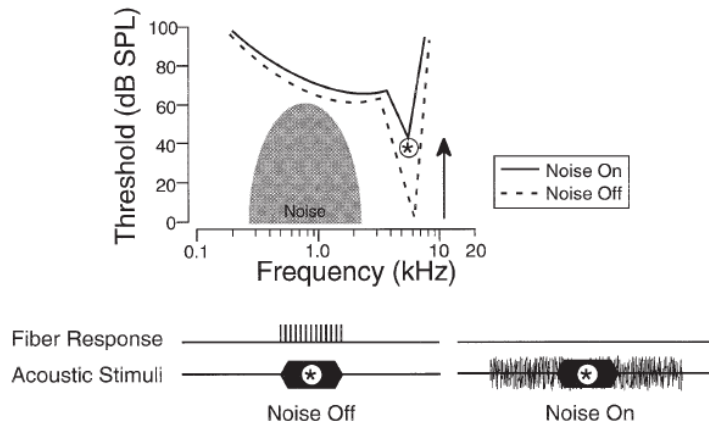


FIGURE 3.10: Suppressive Masking [5]

some mid- to high- frequency sounds. In the proposed MOC model and simulation, the frequency of the target sound is overlapped by the frequency band of the noise, so the target sound should be masked if the noise level is high enough.

3.3.2 Construction of an MOC Model to Simulate the Anti-masking Effect

Chintanpalli et al. [12] have successfully simulated anti-masking effects of the olivocochlear reflex in sustained noise. They used the open-loop model and swept the OHC

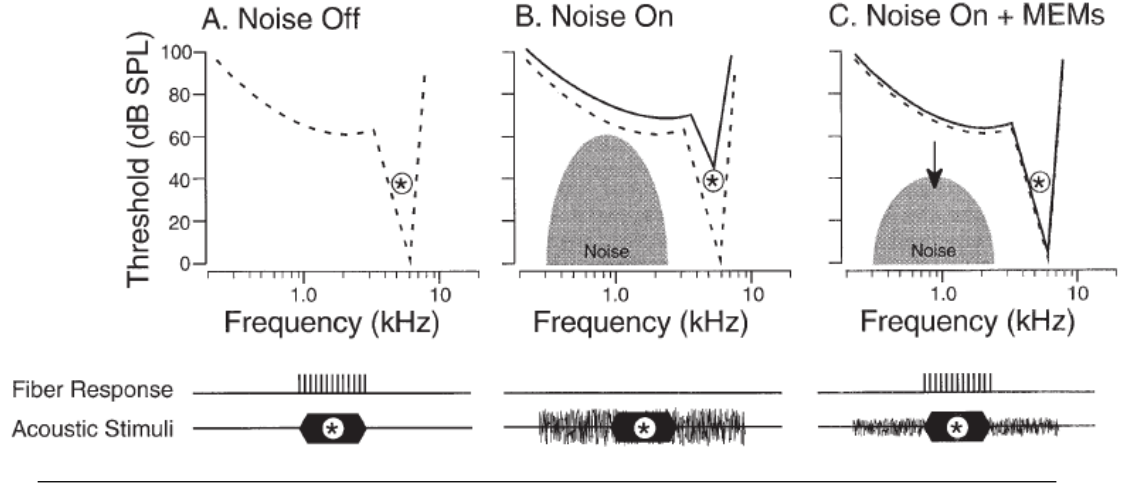


FIGURE 3.11: MEM Anti-Masking [5]

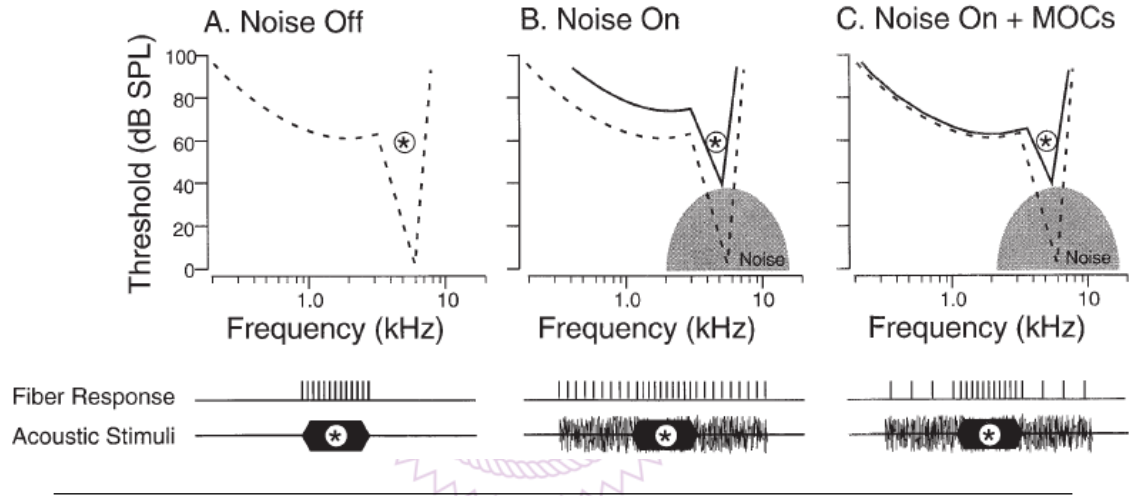


FIGURE 3.12: MOC Anti-Masking [5]

gain by adjusting the capacitance, C_{OHC} . However, according to Housley and Ashmore's experiment results[8], acetylcholine (ACh) makes the OHC conductance to increase, which causes the OHC gain to decrease consequently. This is illustrated in 3.13 [8]; the slope of the current-voltage curve represents the conductance of OHC. With ACh was applied to OHC, the slope increased, which indicates the conductance of OHC increased. OHC is mediated by the MOC interneurons; consequently, it is highly possible that MOC causes conductance of OHC to change rather than capacitance. Hence, based on Housley and Ashmore's experiment results, we proposed a new MOC model which changes the OHC gain by altering the conductance, G_{OHC} , and simulate the closed-loop condition.

The inputs of proposed MOC model are projected from the TM (Figure 3.2) tonotopically, and the MOC outputs mediate the OHC by changing their conductance. The more

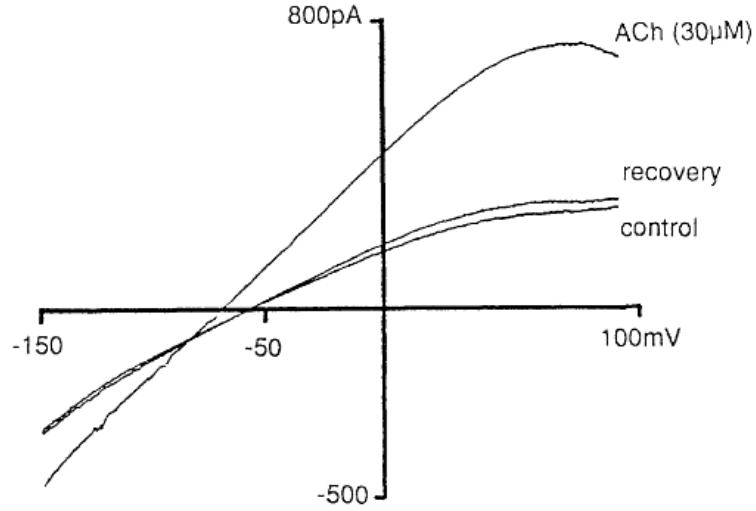


FIGURE 3.13: Outer hair cell responses to ACh [8]

intense the MOC input at specific position index is, the higher the OHC conductance at the corresponding position index is (Figure 3.3). In this manner, the formulated equation is

$$G_{\text{OHC}}(x, t) = G_{0,\text{OHC}}(x) [1 + c_{\text{MOC}} \cdot h_{\text{MOC}}(t) * e_{\text{MOC}}(x, t)], \quad (3.13)$$

where $*$ denote the convolution operator, and $h_{\text{MOC}}(t)$ is a gamma function,

$$h_{\text{MOC}}(t) = \frac{t}{\tau_{\text{MOC}}} e^{-\frac{t}{\tau_{\text{MOC}}}}. \quad (3.14)$$

c_{MOC} is a constant. $G_{0,\text{OHC}}(x)$ is the initial conductance of OHC, when no excitation $e_{\text{MOC}}(x, t)$ presents.

Figure 3.14 is a convolution kernel simulation. According to Oertel et al.'s experiment measurement [32], the firing rate of TM is set to 500 spikes/sec, and the period is 2 ms. The length of convolution kernel $h_{\text{MOC}}(t)$ and input excitation $e_{\text{MOC}}(x, t)$ are 0.5 ms and 1 s respectively, and Figure 3.14 only shows 0.25 ms length. The total convolution output length is 1.5 s. The result shows that with these settings ($\tau_{\text{MOC}} = 0.05$ s for $h_{\text{MOC}}(t)$ and $R_{A,\text{TM}} = 0.75$ ms for $e_{\text{MOC}}(x, t)$), it takes about 200 ms to reach the maximum value, which is the duration MOC takes to achieve its full response. The open-loop simulation increase the conductance for about 1.6 times.

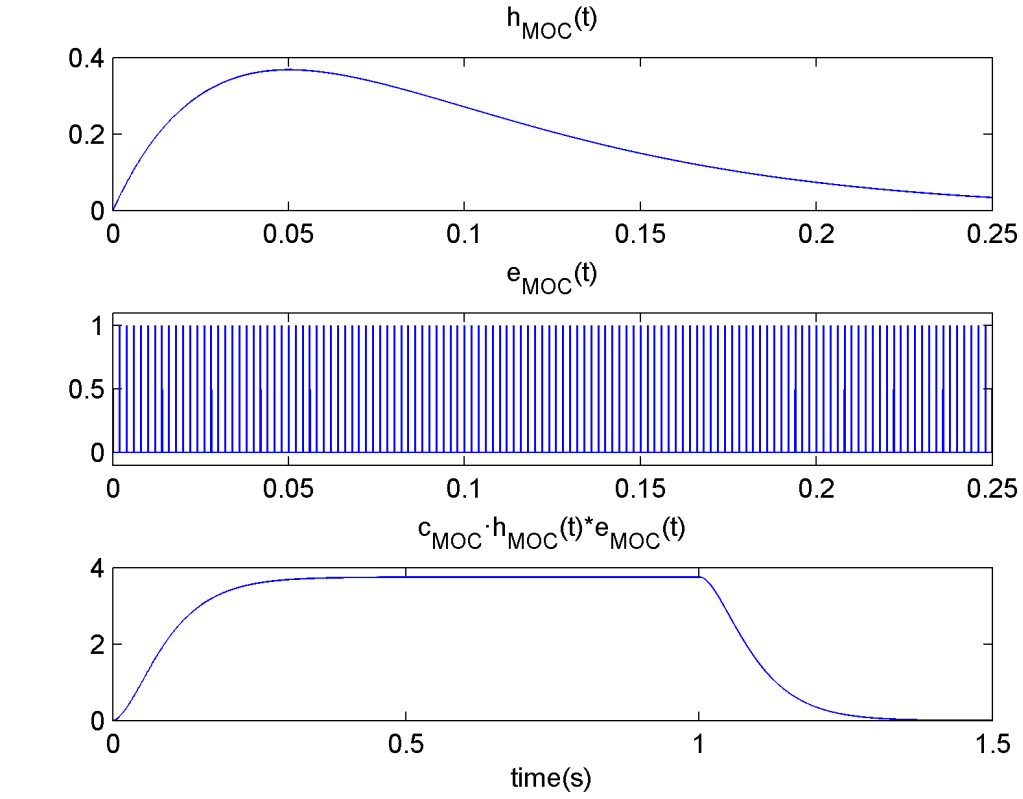


FIGURE 3.14: MOC Convolution Kernel

3.3.3 Experiment Result

The closed-loop anti-masking effect simulation result is the dashed curve with triangle marker shown on Figure 3.5. The MOC close-loop mediation markedly expands the dynamic range from approximately 100 spikes/sec to 200 spikes/sec. The anti-masking effect is notable especially in the low-level region (< 60 dB), and increases the slope in mid-level region (30 - 60 dB). Thence, the different level of sounds are discriminated, which maybe helpful for human to distinguish different sound components.

3.4 The Tuberculoventral Cell

The tuberculoventral (TUB) cell or the vertical cell is located in the deep layer of DCN. It is identified as a kind of type II interneuron, which shows much different characteristics from other interneurons.

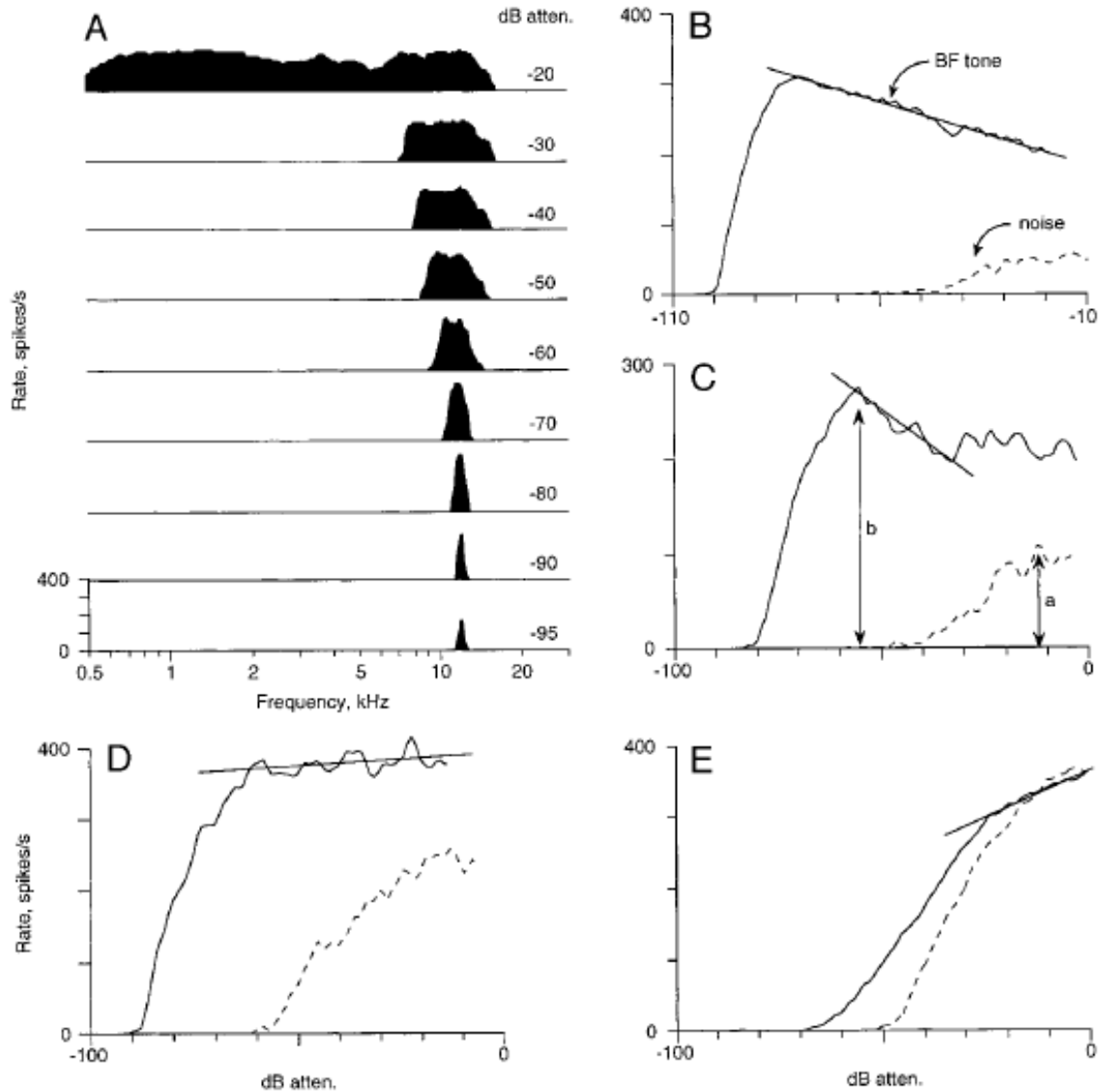


FIGURE 3.15: Tuberculoventral Cell Response Characteristics [9]

Figure 3.15 [9] shows the characteristics of type II interneurons and other type interneurons from Spirou et al.'s experiment results. Figure 3.15 A is a response map of a type II unit (the same as Figure 3.15 B). The stimulation is a 200ms tone burst with different levels, which are from -20 to -95 dB attenuation. 0dB attenuation varies with frequency, and is set to 100dB SPL. The higher the tone level is, the wider the excitatory response region is. Furthermore, the excitatory regions are always centered at the characteristic frequency of the tone burst. Figure 3.15 B and Figure 3.15 C are the rate-level curves of two type II units. The best frequency (BF) tone bursts are represented by solid lines, and the broadband noise bursts are represented by dashed lines. Figure 3.15 D and

Figure 3.15 E are the rate-level curves of the I and type III units respectively. By comparing Figure 3.15 B-E, we can observe that the slope of type II unit becomes negative when the level exceeds some threshold (about -60 to -80 dB attenuation); however, the slope is always positive or flat for type I/III units. There is another important property: the response of the noise for type II units is very low. In contrast, the response is quite high for type I/III units. This major observation is going to be used for constructing the TUB model.

3.4.1 Construction of a TUB Model

According to Wickesberg and Oertel's experiment [33], they used microinjections of glutamate in the DCN to evoke inhibitory postsynaptic potentials (IPSP) in anteroventral cochlear nucleus (AVCN). They found the inhibition of AVCN by DCN is frequency specific, since only the injections along rostrocaudal band in the DCN evoked IPSPs. In addition, the inhibition in the AVCN is delayed by an synaptic delay with respect to the excitation for about 2 ms.

Based on Wickesberg and Oertel's conclusion: the inhibition in the CN is delayed and frequency-specific; therefore, the proposed TUB model should satisfy these two characteristics.

1. Frequency-specification

Frequency-specification or tonotopy is the main feature of auditory system as mentioned. The cochlear nerve excitation directly passes to the CN at the same tonotopic position (Figure 3.3).

2. Delay

The synaptic delay is resolved by using the convolution kernel; Thus, the maximum inhibiting effect will be delayed.

The proposed TUB model is divided into two parts:

1. Inhibiting the TM interneuron in the VCN

By bringing in the delay and frequency-specification properties, the proposed TUB model is constructed and inhibits the TM interneuron.

2. Lateral inhibition

To enhance the frequency-specific property, the lateral inhibition (LI) mechanism is assumed to be applied to the TUB in a way that resembles the visual system[34].

3.4.2 Inhibiting the TM interneuron in the VCN

In order to reduce the discharge rate of TM interneuron, the threshold of TM interneuron to be excited is raised. That is

$$\theta_{\text{TM}}(x, t) = \theta_{0, \text{TM}}(x) \cdot (1 + \text{inh}_{\text{TM}}(x, t)), \quad (3.15)$$

where $\text{inh}_{\text{TM}}(x, t)$ is the inhibiting amount of TUB. The higher $1 + \text{inh}_{\text{TM}}(x, t)$ is, the higher $\theta_{\text{TM}}(x, t)$ is, i.e., TM interneuron is harder to be excited. The delayed inhibition is constructed by importing a convolution kernel.

$$\text{inh}_{\text{TM}} = c_{\text{TUB}} \cdot h_{\text{TUB}}(t) * e_{\text{TUB}}(x, t), \quad (3.16)$$

where

$$h_{\text{TUB}}(t) = \left(\frac{t}{\tau_{\text{TUB}}} e^{-\frac{t}{\tau_{\text{TUB}}}} \right)^5, \quad (3.17)$$

and c_{TUB} is a constant. $e_{\text{TUB}}(x, t)$ is the TUB output. the TUB output will be delayed owing to the convolution kernel to transform into inhibition.

Figure 3.16 is an open-loop TUB convolution kernel simulation results. The TUB convolution kernel scale is much smaller than MOC's ($\tau_{\text{MOC}} = 50$ ms and $\tau_{\text{TUB}} = 2$ ms). It is reasonable because the synaptic delay is much smaller compared to the adaptation of MOC effects. The synaptic delay in this proposed TUB model is about 3 ms, which is closed to Wickesberg and Oertel's experiment result.

3.4.3 Lateral Inhibition

To increase the frequency selectivity of the TUB, LI is introduced into the TUB model. Each TUB will suppress the neighbor TUBs which CF is higher or lower on the tonotopic organization (Figure 3.17). In the tone-only condition, TUB with CF as the tone frequency will dominate and inhibit other TUBs with different CFs; consequently, the

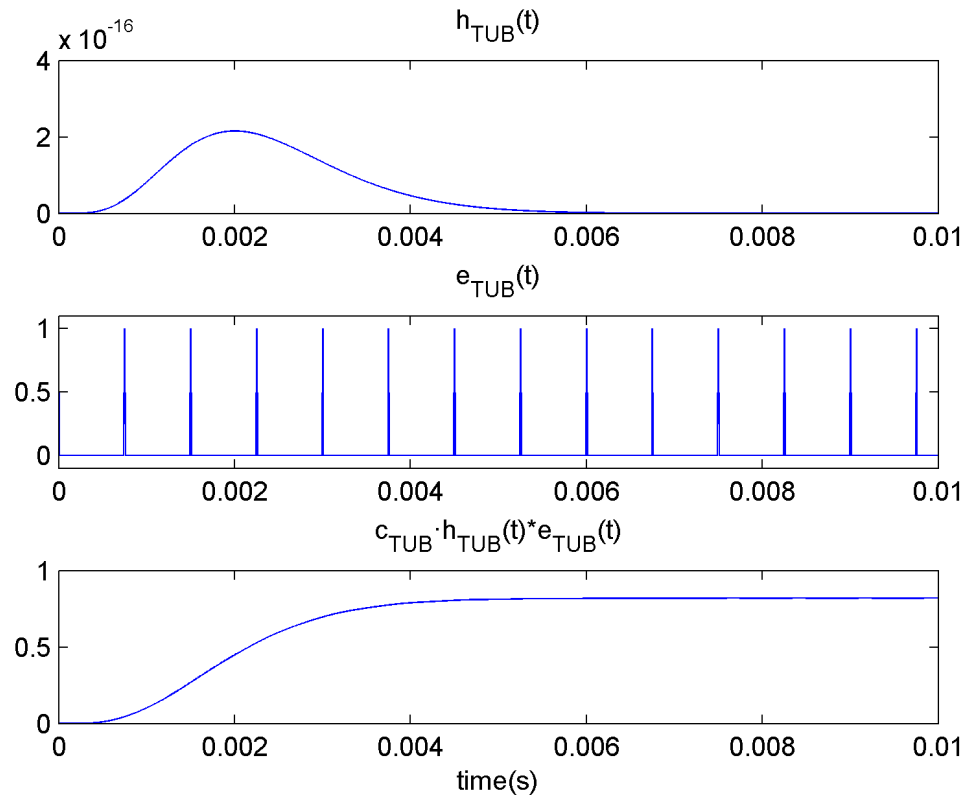


FIGURE 3.16: TUB Convolution Kernel

TUB responds to the tone. On the other hand, in the wide-band-noise condition, because the noise is composed of all the frequency components, TUBs with different CFs suppress one other; therefore, the TUBs do not respond to the noise as much as to the tone. This explains Spirou et al.'s experiment results (Figure 3.15 B and C).

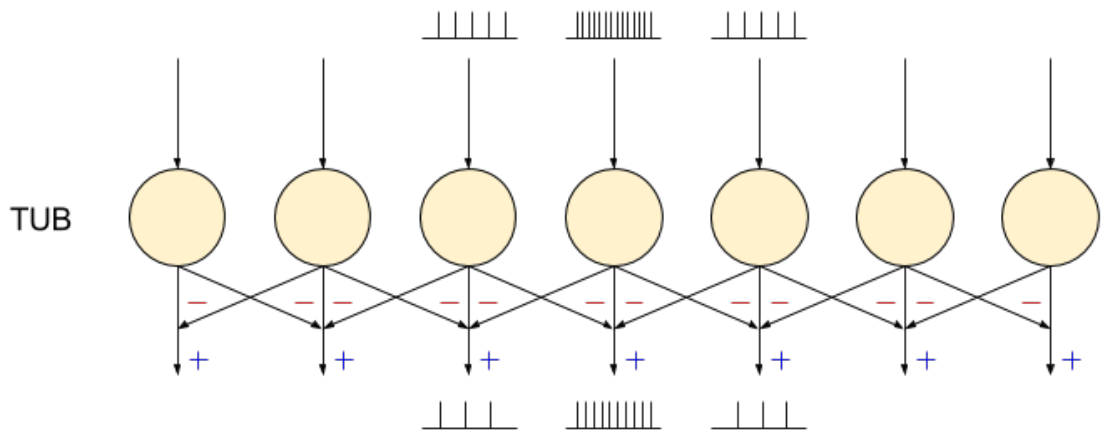


FIGURE 3.17: Lateral Inhibition Diagram

The LI model is constructed by using the same techniques as the inhibition in TM by TUB which raises the TUB threshold potential.

$$\theta_{\text{TUB}}(x, t) = \theta_{0, \text{TUB}}(x) \cdot (1 + \text{inh}_{\text{TUB}}(x, t)), \quad (3.18)$$

where $\text{inh}_{\text{TUB}}(x, t)$ is the inhibiting amount in TUB. Again, the higher $1 + \text{inh}_{\text{TUB}}(x, t)$ is, the harder it is to excite a TUB cell.

$$\text{inh}_{\text{TUB}} = \frac{1}{c_{\text{TUB}}} \cdot h_{\text{TUB}}(t) * e_{\text{TUB}}(x - 1, t) + \frac{1}{c_{\text{TUB}}} \cdot h_{\text{TUB}}(t) * e_{\text{TUB}}(x + 1, t) \quad (3.19)$$

$$= \frac{1}{c_{\text{TUB}}} \cdot h_{\text{TUB}}(t) * [e_{\text{TUB}}(x - 1, t) + e_{\text{TUB}}(x + 1, t)], \quad (3.20)$$

where $e_{\text{TUB}}(x - 1, t)$ represents the excitation of the neighbor TUB whose CF is lower than the TUB at x . Likewise, $e_{\text{TUB}}(x + 1, t)$ represents the excitation of neighbor TUB whose CF is higher than the TUB at x .

3.5 Simulate Sustained Tone-in-Noise Condition

3.5.1 Stimulus Setting

In this section, the stimulus is set to be continuous tone in sustained noise. The tone is a 4000 Hz, 1200 ms sinusoidal wave with variable levels, and the noise is a 55 dB SPL, 1200 ms white noise. The measurement of AN outputs begins at 300 ms and ends at 1200 ms. The tone level is swept from 0 to 100 dB with a 10 dB step. The four conditions: masking, anti-masking, TUB inhibition, and LI are repeated 5 times for each, then the RL graph is plotted.

3.5.2 Experiment Results

As shown in Figure 3.5, both TUB inhibition (with TUB) and LI (with LI) shift the RL curves to the left, compared to RL curves of anti-masking effect (with MOC). Because the TUB causes the target TM to raise its threshold potential, the firing rate of the

TM decreases. And then, the MOC inputs decrease, especially in the tone level ranging between 30 to 50 dB. Hence, the decreasing firing rate in 30 to 50 dB region makes the RL curve seem to slightly shift to left.

With LI, the RL dynamic range slightly increases. Because the LI causes TUBs to be less responsive to noise, the noise background suppresses the TUB inhibition in TMs. The TMs thus deliver more stimulus to MOC, and the dynamic range is increased.

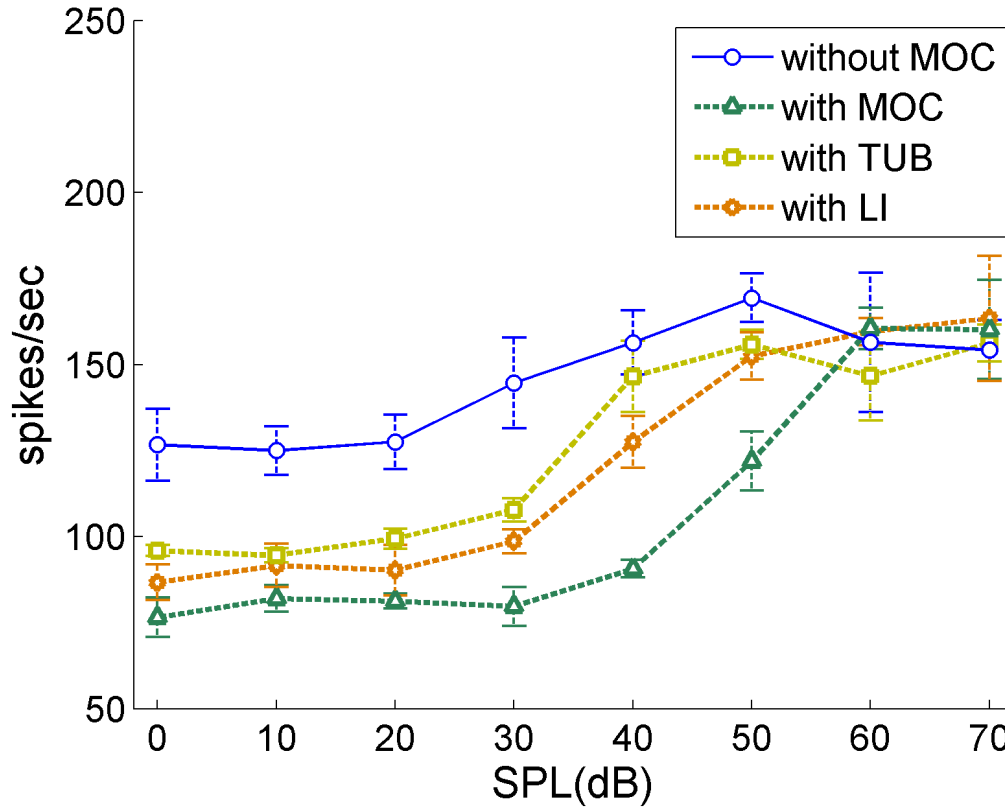


FIGURE 3.18: RL Plot of AN at Sustained Tone in Noise condition

Figure 3.18 is the RL plot of AN for sustained tone-in-noise condition. Comparing the result with Figure 3.5, the dynamic range becomes narrower for all conditions; especially, the firing rate of mid- to high-level (> 60 dB) decreases to about 155 spikes/sec. It is mainly because the sustained tone keeps stimulate the AN. Thus, the neural transmitter for the AN is depleted, and the firing rate declines.

With the MOC, although the dynamic range has been enlarged dramatically, the range of distinguishable tone levels is narrow (30 - 60 dB SPL). In other words, the RLs are about the same between 0 and 30 dB SPL. With TUB and LI, the slope is smoothed and

the range of distinguishable tone levels is widened (20 - 70 dB SPL); also, the dynamic range is kept wide well.



Chapter 4

Conclusion

4.1 Conclusion

The proposed MOC model simulates the anti-masking effect in low tone-level region (< 50 dB), but not obvious in high level region (> 50 dB). Therefore, the auditory discrimination is initially processed in this descending pathway with MOC. The new TUB model is proposed to enhance the sustained tone-in-noise condition. In the tone-burst-in-noise condition, the RL curve with TUB and LI slightly shifts to the left but the range of distinguishable levels is not affected. However, in the sustained tone-in-noise condition, the distinguishable tone levels of RL curve is widened. Therefore, the TUB in DCN may help to make the RL curve smoother, and enhance the discrimination ability of human between different tone levels.

4.2 Future Work

1. Computation time

In the current model structure, all the mechanism are simulated in time domain, and the peripheral pathway are simulated by using differential equations, which makes the calculation too complex. Also, to do the statistics, the simulations are swept from 0 dB to 100 dB with step 10dB, and are repeated 5 times, so there will be total $11 \cdot 5 = 55$ simulations. It always costs days to complete a whole batch. In order to add up other models in the future, the most important object

of simulations is to reduce the calculation complexity. Possible solutions might include simplifying the equation, and adopting probabilistic models.

2. Add other interneurons models in CN

For now, the model only contains TMs in the VCN and TUBs in the DCN, but there are still other functional interneurons in the VCN, e.g., globular bushy cells, spherical bushy cells, and octopus cells. These interneuron models can be contained in the current model to let the model become more complete.

3. Consider other stimulus type and statistics

More complex sound stimulus can be used to see how the AN signal will be affected. Also, except for RL plot, new statistic and plotting techniques can be employed, such as peristimulus time histogram (PSTH) and synchronization index.



Appendix A

Parameters

TABLE A.1: Middle Ear Parameters

| Symbol | Meaning (unit) | Value |
|-------------------------------|--|----------------------|
| Maleus-incus-eardrum | | |
| A_m | Area of eardrum (cm^2) | 0.5 |
| M_m | Effective mass (g) | 8.5×10^{-3} |
| R_m | Effective resistance (g s^{-1}) | 20 |
| K_m | Effective stiffness (g s^{-2}) | 1.5×10^5 |
| g_m | Maleus-incus lever ratio | 0.7 |
| Incudo-stapedial joint | | |
| R_i | Resistance (g s^{-1}) | 400 |
| k_I | Stiffness (g s^{-2}) | 5×10^6 |
| Stapes | | |
| A_s | Area of stapes footplate (cm^2) | 0.0625 |
| M_s | Effective mass (g) | 5×10^{-3} |
| R_s | Effective resistance (g s^{-1}) | 80 |
| K_s | Effective stiffness (g s^{-2}) | 5×10^5 |
| Round-window | | |
| A_r | Area of round window (cm^2) | 0.0625 |
| M_r | Effective mass (g) | 5×10^{-3} |
| R_r | Effective resistance (g s^{-1}) | 20 |
| K_r | Effective stiffness (g s^{-2}) | 1.5×10^5 |

TABLE A.2: Chochlea and OHC Parameters

| Symbol | Meaning (unit) | Base | Mid | Apex |
|--|--|----------------------|----------------------|----------------------|
| Organ of Corti mechanism | | | | |
| M | Mass in OHC load impedance (g) | 2.8×10^{-8} | 5.0×10^{-7} | 2.8×10^{-5} |
| R | Resistance in OHC load impedance (g s^{-1}) | 9.4×10^{-4} | 9.2×10^{-4} | 2.7×10^{-3} |
| K | Stiffness in OHC load impedance (g s^{-2}) | 200 | 11 | 0.76 |
| m | BM mass per unit area (g cm^{-2}) | 3.8×10^{-5} | 2.8×10^{-4} | 2.1×10^{-3} |
| r | BM resistance per unit area ($\text{g s}^{-1} \text{cm}^{-2}$) | 1.5 | 3.2 | 8.6 |
| k | BM stiffness per unit area ($\text{g s}^{-2} \text{cm}^{-2}$) | 5.9×10^5 | 4.0×10^4 | 1.6×10^3 |
| Outer hair cell electromechanical | | | | |
| T | Piezoelectric transformer ratio (m/C) | 2.4×10^6 | 2.4×10^6 | 2.4×10^6 |
| G | Membrane conductance (nS) | 91 | 51 | 33 |
| C | Membrane capacitance (pF) | 14 | 32 | 79 |
| C_g | Gating capacitance (pF) | 18 | 33 | 70 |
| α_d | MET's sensitivity to RL ¹ displacement (A/m) | 1.6×10^{-3} | 6.2×10^{-4} | 2.0×10^{-4} |
| α_v | MET's sensitivity to RL velocity (C/m) | 4.4×10^{-6} | 1.8×10^{-6} | 6.8×10^{-7} |
| I_{\max} | Maximum range of OHC receptor current (pA) | 670 | 320 | 83 |
| Physical dimensions | | | | |
| A | Cochlear corss-sectional area (cm^2) | 3.8×10^{-5} | 3.8×10^{-5} | 3.8×10^{-5} |
| w | BM width (cm) | 0.031 | 0.04 | 0.051 |
| L | Length of cochlea (cm) | | 3.5 | |

TABLE A.3: IHC Parameters

| Symbol | Meaning (unit) | Value |
|---|--|---|
| IHC receptor potential | | |
| E_t | Endocochlear potential (V) | 100×10^{-3} |
| E_k | Potassium reversal potential (V) | -70.45×10^{-3} |
| G_0 | Resting conductance (S) | 1.974×10^{-9} |
| G_k | Potassium conductance (S) | 1.8×10^{-8} |
| $R_p / (R_t + R_p)$ | E_k correlation | 0.04 |
| $G_{\text{cilia}}^{\text{max}}$ | Maximum mechanical conductance | 8×10^{-9} |
| s_0 | Displacement sensitivity (m^{-1}) | 85×10^{-9} |
| u_0 | Displacement offset (m) | 7×10^{-9} |
| s_1 | Displacement sensitivity (m^{-1}) | 5×10^{-9} |
| u_1 | Displacement offset (m) | 7×10^{-9} |
| C_m | Total capacitance (s) | 6×10^{-12} |
| τ_c | Cilia/BM time constant (s) | 2.13×10^{-3} |
| C_{cilia} | Cilia/BM coupling gain (dB) | 16 |
| IHC synapse calcium channels | | |
| z | Scalar factor ($s \cdot [\text{Ca}^{2+}]^3$) ⁻¹ | 20×10^{31} |
| E_{Ca} | Reversal potential (V) | 0.066 |
| β_{Ca} | $m_{I_{\text{Ca}},\infty}$ constant | 400 |
| γ_{Ca} | $m_{I_{\text{Ca}},\infty}$ constant | 130 |
| τ_m | Calcium current time constant (s) | 1×10^{-4} |
| τ_{Ca} | Calcium diffusion time constant (s) | 1×10^{-4} |
| Transmitter release | | |
| y | Replenishment rate (s^{-1}) | 10 |
| l | Loss rate (s^{-1}) | 2580 |
| x | Reprocessing rate (s^{-1}) | 66.3 |
| r | Recovery rate (s^{-1}) | 6580 |
| Initial value of state variables | | |
| k_0 | Release rate initial value | 32.7869 |
| c | Vesicle numbers of cleft | $k_0 \cdot y \cdot M / (y \cdot (l + r) + k_0 \cdot l)$ |
| q | Vesicle numbers of free transmitter pool | $c \cdot (l + r) / k_0$ |
| w | Vesicle numbers of reproccsing store | $c \cdot r / x$ |

TABLE A.4: AN Parameters

| Symbol | Meaning (unit) | H1 | H2 | M1 | M2 | L1 | L2 |
|------------------------------------|--|----|-----|----|----|------|-----|
| Fiber type | | | | | | | |
| $G_{\text{Ca}}^{\text{max}}$ | Maximum Ca^{2+} conductance (nS) | 27 | 13 | 12 | 11 | 2.8 | 2 |
| $[\text{Ca}^{2+}]_{\text{thr}}$ | Threshold of Ca^{2+} concentration | 16 | 1.6 | 7 | 6 | 1.6 | 1.2 |
| M | Maximum free transmitter quanta | 12 | 9 | 11 | 15 | 8 | 7 |
| Action potential generation | | | | | | | |
| c_r | Maximum contribution of the relative refractory period | | | | | 0.55 | |
| s_r | Time constant of refraction (ms) | | | | | 0.8 | |
| R_A | Absolute refractory period (ms) | | | | | 0.75 | |

TABLE A.5: TM Cell Parameters

| Symbol | Meaning (unit) | Value |
|------------------------|--|-------|
| Dendrite | | |
| N | Number of auditory nerve fibers | 5 |
| f_c | Cut-off frequency (Hz) | 500 |
| I_{\max} | Maximum current that could be delivered to the soma (nA) | 7.5 |
| Soma | | |
| c | Accommodation constant | 0 |
| τ_{TH} | Time constant of threshold rise (ms) | 20 |
| b | Delayed rectifier potassium conductance strength (nS) | 500 |
| τ_{G_k} | Time constant of potassium conductance decay (ms) | 0.35 |
| $\theta_{0,\text{TM}}$ | Resting threshold of the cell (mV) | 2 |
| τ_m | Membrane time constant (ms) | 2 |
| R_i | Input resistance ($\text{M}\Omega$) | 60 |
| E_b | Reversal potential (mV) | 50 |
| E_0 | Resting membrane potential soma (mV) | -10 |
| E_k | Equilibrium potential of potassium conductance (mV) | -60 |
| $R_{A,\text{TM}}$ | Absolute refractory period (ms) | 0.75 |

TABLE A.6: TUB Cell Parameters

| Symbol | Meaning (unit) | Value |
|-------------------------|--|-------|
| Dendrite | | |
| N | Number of auditory nerve fibers | 30 |
| f_c | Cut-off frequency (Hz) | 5000 |
| I_{\max} | Maximum current that could be delivered to the soma (nA) | 24 |
| Soma | | |
| c | Accommodation constant | 0 |
| τ_{TH} | Time constant of threshold rise (ms) | 20 |
| b | Delayed rectifier potassium conductance strength (nS) | 4000 |
| τ_{G_k} | Time constant of potassium conductance decay (ms) | 0.35 |
| $\theta_{0,\text{TUB}}$ | Resting threshold of the cell (mV) | 3 |
| τ_m | Membrane time constant (ms) | 2 |
| R_i | Input resistance ($\text{M}\Omega$) | 60 |
| E_b | Reversal potential (mV) | 50 |
| E_0 | Resting membrane potential soma (mV) | -10 |
| E_k | Equilibrium potential of potassium conductance (mV) | -60 |
| $R_{A,\text{TUB}}$ | Absolute refractory period (ms) | 0.75 |

TABLE A.7: Convolution Kernel Parameters

| Symbol | Meaning (unit) | Value |
|---------------------|---------------------------------------|-----------------------|
| MOC | | |
| τ_{MOC} | Time constant of kernel function (ms) | 50 |
| c_{MOC} | Scalar factor of of kernel function | 0.15 |
| TUB | | |
| τ_{TUB} | Time constant of kernel function (ms) | 3 |
| c_{TUB} | Scalar factor of of kernel function | 1.25×10^{15} |

Appendix B

State-space Formulation of Liu and Neely Model

This appendix is mainly to derive the state equations of Liu and Neely equations in section 2.3.6. By using the state-space equations, we only need to give six state variables to derive other cochlear and OHC variables. It simplifies the equations and is convenient to be employed to the computer program.

B.1 Equation (2.19)

$$\boxed{\xi_o = TQ} \tag{B.1}$$

$$\rightarrow \dot{\xi}_o = T\dot{Q} \tag{B.2}$$

$$\rightarrow \dot{Q}(x) = T^{-1}u_o \tag{B.3}$$

B.2 Equation (2.22)

$$i_r(u_r, \xi_r) = GV + C\dot{V} + \dot{Q} \tag{B.4}$$

$$= GV + C\dot{V} + T^{-1}u_o \tag{B.5}$$

$$\rightarrow \dot{V}(x) = \frac{1}{C}(i_r(u_r, \xi_r) - GV - T^{-1}u_o) \tag{B.6}$$

B.3 Equation (2.21)

$$\boxed{\tilde{V} = V - T f_{OHC}} \quad (\text{B.7})$$

$$\rightarrow f_{OHC} = \frac{V - \tilde{V}}{T} \quad (\text{B.8})$$

$$= \frac{V - C_g^{-1}Q}{T} \quad (\text{B.9})$$

$$\boxed{f_{OHC} = M\ddot{\xi}_o + R\dot{\xi}_o + K\xi_o} \quad (\text{B.10})$$

$$\rightarrow \ddot{\xi}_o = \frac{f_{OHC} - R\dot{\xi}_o - K\xi_o}{M} \quad (\text{B.11})$$

$$= \frac{-R\dot{\xi}_o - K\xi_o}{M} + \frac{f_{OHC}}{M} \quad (\text{B.12})$$

$$= \frac{-R\dot{\xi}_o - K\xi_o}{M} + \frac{V - C_g^{-1}Q}{TM} \quad (\text{B.13})$$

$$\rightarrow \ddot{u}_o(x) = -\frac{Ru_o + KTQ}{M} + \frac{V - C_g^{-1}Q}{TM} \quad (\text{B.14})$$

B.4 Equation (2.20)

$$\boxed{\xi_b = \xi_r + \xi_o} \quad (\text{B.15})$$

$$\rightarrow \xi_r = \xi_b - \xi_o \quad (\text{B.16})$$

$$\boxed{m\ddot{\xi}_b + r\dot{\xi}_b + k\xi_b = -P} \quad (\text{B.17})$$

$$\ddot{\xi}_b = \frac{-r\dot{\xi}_b - k\xi_b - P(x)}{m} \quad (\text{B.18})$$

$$= \frac{-r(\dot{\xi}_r + \dot{\xi}_o) - k(\xi_r + \xi_o) - P(x)}{m} \quad (\text{B.19})$$

$$= -\frac{r(u_r + u_o) + k(\xi_r + TQ)}{m} - \frac{P(x)}{m} \quad (\text{B.20})$$

$$\rightarrow \ddot{u}_o = \ddot{\xi}_r \quad (\text{B.21})$$

$$= \ddot{\xi}_b - \ddot{\xi}_o \quad (\text{B.22})$$

$$= \frac{Ru_o + KTQ}{M} - \frac{V - C_g^{-1}Q}{TM} - \frac{r(u_r + u_o) + k(\xi_r + TQ)}{m} - \frac{P(x)}{m} \quad (\text{B.23})$$



Bibliography

- [1] Y.-W. Liu and S. T. Neely, “Outer hair cell electromechanical properties in a nonlinear piezoelectric model,” *The Journal of the Acoustical Society of America*, vol. 126, pp. 751–761, Aug. 2009.
- [2] Y.-W. Liu and S. T. Neely, “Distortion product emissions from a cochlear model with nonlinear mechanoelectrical transduction in outer hair cells,” *The Journal of the Acoustical Society of America*, vol. 127, pp. 2420–2432, Apr. 2010.
- [3] C. J. Sumner, E. A. Lopez-Poveda, L. P. O’Mard, and R. Meddis, “A revised model of the inner-hair cell and auditory-nerve complex,” *The Journal of the Acoustical Society of America*, vol. 111, pp. 2178–2188, May 2002.
- [4] M. J. Hewitt, R. Meddis, and T. M. Shackleton, “A computer model of a cochlear-nucleus stellate cell: responses to amplitude-modulated and pure-tone stimuli,” *The Journal of the Acoustical Society of America*, vol. 91, pp. 2096–2109, Apr. 1992.
- [5] M. C. Liberman and J. J. Guinan, “Feedback control of the auditory periphery: anti-masking effects of middle ear muscles vs. olivocochlear efferents,” *Journal of communication disorders*, vol. 31, no. 6, 1998.
- [6] L. R. Squire, *Chap. 26 Audition*, ch. 26. Elsevier / Academic Press, 3 ed., Feb. 2008.
- [7] E. D. Young and D. Oertel, *Chap. 4 The cochlear nucleus*, vol. 5, ch. Introduction to Synaptic Circuits. Oxford University Press, 2004.
- [8] G. D. Housley and J. F. Ashmore, “Direct measurement of the action of acetylcholine on isolated outer hair cells of the guinea pig cochlea,” *Proceedings: Biological Sciences*, vol. 244, pp. 161–167, May 1991.

- [9] G. A. Spirou, K. A. Davis, I. Nelken, and E. D. Young, "Spectral integration by type II interneurons in dorsal cochlear nucleus.," *Journal of neurophysiology*, vol. 82, pp. 648–663, Aug. 1999.
- [10] L.-M. Yu, "Establishing a biophysical auditory model from middle ear to brainstem and simulating the unmasking response of cochlea by delayed, frequency specific tuberculoventral inhibition," Master's thesis, National Tsing Hua University, July 2012.
- [11] T. Kawase, B. Delgutte, and M. C. Liberman, "Antimasking effects of the olivocochlear reflex. II. enhancement of auditory-nerve response to masked tones.," *Journal of neurophysiology*, vol. 70, pp. 2533–2549, Dec. 1993.
- [12] A. Chintanpalli, S. G. Jennings, M. G. Heinz, and E. A. Strickland, "Modeling the anti-masking effects of the olivocochlear reflex in auditory nerve responses to tones in sustained noise.," *Journal of the Association for Research in Otolaryngology : JARO*, vol. 13, pp. 219–235, Apr. 2012.
- [13] A. L. Hodgkin and A. F. Huxley, "A quantitative description of membrane current and its application to conduction and excitation in nerve.," *The Journal of physiology*, vol. 117, pp. 500–544, Aug. 1952.
- [14] J. Matthews, "Modeling reverse middle ear transmission of acoustic distortion signals," in *Mechanics of Hearing* (E. de Boer and M. A. Viergever, eds.), pp. 11–18+, Springer Netherlands, 1983.
- [15] R. Meddis, L. P. O'Mard, and E. A. Lopez-Poveda, "A computational algorithm for computing nonlinear auditory frequency selectivity.," *The Journal of the Acoustical Society of America*, vol. 109, pp. 2852–2861, June 2001.
- [16] R. Meddis, "Simulation of mechanical to neural transduction in the auditory receptor.," *The Journal of the Acoustical Society of America*, vol. 79, pp. 702–711, Mar. 1986.
- [17] T. A. Ghanem, K. D. Breneman, R. D. Rabbitt, and H. M. Brown, "Ionic composition of endolymph and perilymph in the inner ear of the oyster toadfish, *Opsanus tau*.," *The Biological bulletin*, vol. 214, pp. 83–90, Feb. 2008.

- [18] S. A. Shamma, R. S. Chadwick, W. J. Wilbur, K. A. Morrish, and J. Rinzel, "A biophysical model of cochlear processing: intensity dependence of pure tone responses.," *The Journal of the Acoustical Society of America*, vol. 80, pp. 133–145, July 1986.
- [19] D. C. Mountain and A. E. Hubbard, "Computational analysis of hair cell and auditory nerve processes," in *Auditory Computation* (H. Hawkins, T. McMullen, A. Popper, and R. Fay, eds.), vol. 6 of *Springer Handbook of Auditory Research*, pp. 121–156+, Springer New York, 1996.
- [20] A. J. Hudspeth and R. S. Lewis, "Kinetic analysis of voltage- and ion-dependent conductances in saccular hair cells of the bull-frog, *rana catesbeiana*.,," *The Journal of physiology*, vol. 400, pp. 237–274, June 1988.
- [21] R. C. Kidd and T. F. Weiss, "Mechanisms that degrade timing information in the cochlea.," *Hearing research*, vol. 49, pp. 181–207, Nov. 1990.
- [22] G. J. Augustine, M. P. Charlton, and S. J. Smith, "Calcium entry and transmitter release at voltage-clamped nerve terminals of squid.," *The Journal of physiology*, vol. 367, pp. 163–181, Oct. 1985.
- [23] J. H. Siegel, "Spontaneous synaptic potentials from afferent terminals in the guinea pig cochlea.," *Hearing research*, vol. 59, pp. 85–92, Apr. 1992.
- [24] M. R. Schroeder, B. S. Atal, and J. L. Hall, "Optimizing digital speech coders by exploiting masking properties of the human ear," *The Journal of the Acoustical Society of America*, vol. 66, pp. 1647–1652, Dec. 1979.
- [25] E. Zwicker and H. Fastl, *Psychoacoustics: Facts and Models (Springer Series in Information Sciences) (v. 22)*. Springer, 2nd updated ed. ed., Apr. 1999.
- [26] N. B. Cant, "The fine structure of two types of stellate cells in the anterior division of the anteroventral cochlear nucleus of the cat.," *Neuroscience*, vol. 6, no. 12, pp. 2643–2655, 1981.
- [27] W. S. Rhode and P. H. Smith, "Encoding timing and intensity in the ventral cochlear nucleus of the cat.," *Journal of neurophysiology*, vol. 56, pp. 261–286, Aug. 1986.

- [28] W. Rall, "Cable theory for dendritic neurons," in *Methods in Neuronal Modeling* (C. Koch and I. Segev, eds.), ch. Cable Theory for Dendritic Neurons, pp. 9–92, Cambridge, MA, USA: MIT Press, 1989.
- [29] J. J. Guinan, "Olivocochlear efferents: anatomy, physiology, function, and the measurement of efferent effects in humans," *Ear and hearing*, vol. 27, pp. 589–607, Dec. 2006.
- [30] D. E. Vetter, M. C. Liberman, J. Mann, J. Barhanin, J. Boulter, M. C. Brown, J. Saffioti-Kolman, S. F. Heinemann, and A. B. Elgoyhen, "Role of $\alpha 9$ nicotinic ACh receptor subunits in the development and function of cochlear efferent innervation," *Neuron*, vol. 23, pp. 93–103, May 1999.
- [31] J. J. Guinan, "Physiology of olivocochlear efferents," in *The Cochlea* (P. Dallos, A. Popper, and R. Fay, eds.), vol. 8 of *Springer Handbook of Auditory Research*, pp. 435–502+, Springer New York, 1996.
- [32] D. Oertel, S. Wright, X.-J. J. Cao, M. Ferragamo, and R. Bal, "The multiple functions of t stellate/multipolar/chopper cells in the ventral cochlear nucleus," *Hearing research*, vol. 276, pp. 61–69, June 2011.
- [33] R. E. Wickesberg and D. Oertel, "Delayed, frequency-specific inhibition in the cochlear nuclei of mice: a mechanism for monaural echo suppression," *The Journal of neuroscience : the official journal of the Society for Neuroscience*, vol. 10, pp. 1762–1768, June 1990.
- [34] S. L. Macknik and S. Martinez-Conde, *Lateral Inhibition*, ch. 3, pp. 523–525. Sage Publications, 2010.